The Meteoritical Society

Meteoritics & Planetary Science 1–23 (2024)
doi: 10.1111/maps.14261

Early fluid migration and alteration fronts in the CM chondrite Reckling Peak 17085

A. MUSOLINO [1,2]*, M. D. SUTTLE [1,3], L. FOLCO [1,4], A. J. KING [5], G. POGGIALI [6,7], H. C. BATES [5], J. R. BRUCATO [6], and A. BREARLEY [8]

[1]Dipartimento di Scienze della Terra, Università di Pisa, Pisa, Italy
[2]Aix-Marseille Université, CEREGE, CNRS, IRD, Aix-en-Provence, France
[3]School of Physical Sciences, The Open University, Walton Hall, Milton Keynes, UK
[4]CISUP, Centro per l'Integrazione della Strumentazione dell'Università di Pisa, Pisa, Italy
[5]Planetary Materials Group, Natural History Museum, London, UK
[6]INAF-Astrophysical Observatory of Arcetri, Florence, Italy
[7]LESIA-Observatoire de Paris, PSL University, Paris, France
[8]UNM, Earth and Planetary Sciences, University of New Mexico, Albuquerque, New Mexico, USA

***Correspondence**
A. Musolino, Dipartimento di Scienze della Terra, Università di Pisa, Pisa 56126, Italy.
Email: musolino@cerege.fr

(Received 31 January 2024; revision accepted 19 August 2024)

Abstract–Reckling Peak (RKP) 17085 is a newly classified Antarctic CM chondrite that preserves a complex alteration history characterized by mild aqueous alteration (CM2.7), overprinted by a short-lived thermal metamorphic event (heating stage III [<750°C]), and affected by low-grade terrestrial weathering. This meteorite contains abundant Fe-rich bands within the fine-grained matrix, composed of micron-scale Fe-oxyhydroxide minerals. They are interpreted as "alteration fronts" arising due to the dissolution and transport of Fe (typically <500 μm) before being abruptly deposited. This alteration texture is relatively rare among hydrated carbonaceous chondrites, with only five reported instances to date (Murchison, Murray, Allan Hills 81002, Miller Range 07687, and Northwest Africa 5958). Evidence from RKP 17085 suggests that early aqueous alteration operated as multiple geochemically isolated microenvironments, which moved outwards from local point sources within the matrix. Low permeability fine-grained rims on chondrules appear to have acted as barriers to fluid flow, controlling the migration of fluid across the parent body. Furthermore, the higher porosity regions within the altered fine-grained matrix represent either void space generated by the dehydration of hydrated minerals during post-hydration metamorphism and/or sites of ice accretion (water-ice or C-bearing ices) preserved within a mildly altered primitive matrix.

INTRODUCTION

Members of the Mighei-type "CM" chondrites are among the most numerous carbonaceous chondrites (735 meteorites as of 29/08/2023, pairings included; The Meteoritical Bulletin, 2023). They sample primitive solar system materials (Brearley et al., 2006; Brearley & Jones, 1998) which contain abundant water and organic matter (e.g., Alexander et al., 2012; Martins, 2011; Trigo-Rodríguez et al., 2019). The CM chondrites are, therefore, of astrobiological interest as potential sources of water (e.g., King et al., 2022) and prebiotic molecules delivered to the terrestrial planets (e.g., Alexander et al., 2017).

The parent bodies of CMs are considered to be C-complex asteroids, based on their similar spectroscopic characteristics (e.g., Bates et al., 2020; Burbine et al., 2002). These are small, primitive solar system bodies that experienced aqueous alteration, sometimes thermal metamorphism, and are almost always brecciated (e.g., Lentfort et al., 2021; Suttle, King, et al., 2021). Aqueous alteration on the CM parent body(ies) was heterogeneous,

meaning that different meteorites record a range of alteration extents, allowing the progression of fluid–rock interaction to be reconstructed. Varying degrees of aqueous alteration led to the transformation of the accretionary anhydrous phases to hydrated and oxidized mineral assemblages (Brearley & Jones, 1998; Howard et al., 2009, 2011; Rubin et al., 2007; Zolensky et al., 1997). This progressive transformation can be quantified using scales based on different analytical techniques: (i) petrographic and mineralogic criteria, considering together the Mineralogical Alteration Index (as a way to monitor substitutions between Fe-cronstedtite and Mg-serpentine), the volume of isolated silicates, and the volume of altered chondrules (Browning et al., 1996); (ii) qualitative petrologic criteria, considering the abundance of phyllosilicates and tochilinite–cronstedtite intergrowths (TCIs), the degree of alteration of phenocrysts and mesostasis in chondrules, oxidation of FeNi metals, the composition of poorly characterized phases (namely TCIs), and carbonate mineralogy (Rubin et al., 2007); (iii) quantitative mineralogic criteria, using position-sensitive detector X-ray diffraction (PSD-XRD), considering the ratio between anhydrous and hydrous silicates (Howard et al., 2009, 2011, 2015); (iv) infrared (IR) spectral features, such as the position of the 3-μm band center related to -OH/H_2O (Beck et al., 2010, 2018; Takir et al., 2013); (v) the degree of hydration, that is, the wt% H in water and OH, or the H and N elemental and isotopic composition for unheated CMs (Alexander et al., 2013).

Most of the CMs are dominated by aqueous alteration products including phyllosilicates (e.g., serpentines), Fe sulfides (pyrrhotite, pentlandite, tochilinite), magnetite, carbonates (e.g., aragonite, calcite, dolomite), Fe-oxyhydroxides and halides (Brearley et al., 2006). Using petrologic criteria, Rubin et al. (2007) classified CM chondrites as subtypes 2.6–2.0, with the recent characterization of minimally aqueously altered CMs extending the classification scheme to subtypes 2.7–3.0 (Hewins et al., 2014; Kimura et al., 2020; Lentfort et al., 2021; Leroux et al., 2015; Marrocchi et al., 2014; Rubin, 2015). The discovery of minimally altered CMs has also reinforced the debate on the relationship between CM and CO (Ornans-type) chondrites, which sometimes share overlapping O-isotopic compositions (Greenwood et al., 2023; Hewins et al., 2014; Kimura et al., 2020).

Some CM meteorites also record post-hydration thermal metamorphism (e.g., King, Mason, et al., 2021; King, Schofield, & Russell, 2021; Nakamura, 2005; Tonui et al., 2014), causing modifications to their original texture and mineralogical composition, and organic, spectral, and isotopic properties. These include, for example, the partial dehydration and recrystallization of phyllosilicates to highly disordered materials and a groundmass of nanoscale olivine (Suttle, King, et al., 2021), the degradation/graphitization of insoluble organic matter (IOM; e.g., Chan et al., 2019), a depletion in water and other volatiles (Alexander et al., 2013), the broadening and increasing symmetry of the 3-μm band that is centered at longer wavelengths, the sharpening of the profile of the 9–12 μm (Si-O) stretching band (more overlapped bands) (Hanna et al., 2020; King, Schofield, & Russell, 2021), the enrichment in heavy oxygen isotopic composition (Clayton & Mayeda, 1999; Lindgren et al., 2020). These overprints make the classification and the reconstruction of the geological history of their parent body complicated (e.g., King, Schofield, & Russell, 2021; Krietsch et al., 2021), leading sometimes to the misclassification of the aqueous alteration level. Differently from anhydrous asteroids for which ^{26}Al is considered the main heat source (McSween Jr et al., 1988), thermal metamorphism in CMs is generally considered short-lived and associated with impacts or solar radiation processes (Amsellem et al., 2020; Nakato et al., 2008; Quirico et al., 2018). Supporting the short-term heating duration in CMs are: (1) physical limitations like the large latent heat and heat capacity of water and heat dissipation that would result from hydrothermal convection (Grimm & McSween Jr., 1989); (2) analytical observations like the different structures of IOM in strongly heated CMs compared to type-3 chondrites (Quirico et al., 2018); (3) ^{87}Rb-^{87}Sr chronology that dates CMs thermal metamorphism 3 Ga after the formation of the solar system (after the complete decay of ^{26}Al at <10 Ma; Amsellem et al., 2020).

The collection of new "falls" such as Winchcombe (King et al., 2022; Suttle, Daly, et al., 2023) and the characterization of CMs in our existing collections plays a fundamental role in understanding the early solar system. Indeed, the large diversity of these meteorites potentially reflects the sampling of multiple parent bodies and different styles of aqueous and/or thermal alteration. However, for "finds", it is necessary to take into account the inevitable overprint of terrestrial weathering, which easily affects the mineralogy of meteorites left in the Earth's environment, especially for CMs (Bland et al., 2006; Jenkins et al., 2023; Lee et al., 2021; Lee & Bland, 2004; Vacher et al., 2020). Weathering fills voids and replaces extraterrestrial mineralogy with secondary minerals as a result of oxidation (e.g., formation of veins). For meteorites collected in Antarctica, the cold and dry polar climate slows the rate of terrestrial alteration (compared to weathering in humid environments at lower latitudes), but even these meteorites do not escape modification to some extent: cryofracturing and deposition of evaporites and iron oxyhydroxide phases (Jull et al., 1988; Velbel, 1988), depletion of highly fluid mobile elements like K, Na, and Rb (Braukmüller et al., 2018), and contamination with terrestrial organic compounds

TABLE 1. Summary of carbonaceous chondrites with alteration fronts and/or aureoles. Petrologic subtypes are indicated using the Rubin et al. (2007) scale (and the extensions of Rubin, 2015 and Kimura et al., 2020 for RKP 17085).

Name	Section	Find/ Fall	Location	Group	Petrologic type	Reference(s)
Murray	UNM 552	Fall	United States	CM	2.4/2.5[a]	Hanowski and Brearley (2000)
Murchison	UNM 640, 641	Fall	Victoria, Australia	CM	2.5[a]	Hanowski and Brearley (2000)
ALH(A) 81002	I3-2, A-2, B-1	Find	Allan Hills, Antarctica	CM	2.2[b]	Hanowski and Brearley (2000, 2001)
NWA 5958	NWA 5958-1	Find	Morocco, Africa	C2-ung (originally CO3)	2.5[a]	Jacquet et al. (2016)
MIL 07687	MIL 07687,4	Find	Miller Range, Antarctica	CO (originally C3-ung)	3	Haenecour et al. (2020), Brearley (2012), Prestgard et al. (2021)
RKP 17085	RKP 1708500, 02	Find	Reckling Peak, Antarctica	CM	2.7	This work

[a]Rubin et al. (2007).
[b]Converted to Rubin's scale from Howard et al. (2015) classification (subtype 1.4).

progressively modify the extraterrestrial signatures of Antarctic meteorites.

This study focuses on a newly recovered Antarctic CM chondrite—Reckling Peak (RKP) 17085. We studied this sample's petrography, bulk O-isotope composition, volatile abundance, IR spectroscopic signature, and organic matter content, providing insights into the complex alteration history of its parent body. RKP 17085 is unbrecciated (at the scale studied [cm]), mildly aqueously altered, and affected by post-hydration thermal metamorphism. The most unusual feature of this sample is the presence of "alteration fronts"—thin Fe-rich bands with sinuous profiles that occur abundantly within the fine-grained matrix. Features fitting this description were first reported within CM chondrites by Hanowski and Brearley (2000), who described them as "aureoles" (Table 1). They were interpreted as the mobilization of Fe from altered metal grains (forming poorly crystalline intermixed TCIs). The Fe-rich fronts and aureoles were considered characteristic of in situ aqueous alteration on the CM chondrite's parent body, in contrast to pre-accretional models for aqueous alteration on CM chondrites (Hanowski & Brearley, 2000, 2001). However, terrestrial alteration was not considered as a potential agent for the formation of the aureoles/fronts. More recently, alteration fronts have been reported in the CO3 chondrite Miller Range (MIL) 07687 (Brearley, 2012; Haenecour et al., 2020; Prestgard et al., 2021) and the C2-ungrouped chondrite Northwest Africa (NWA) 5958 (Jacquet et al., 2016). Another example of aqueous flow features in CM chondrites is documented in the CM1 Meteorite Hills (MET) 01070. In this chondrite, 60- to 1000-μm-thick bands that enclose centimeter-sized lenses and enriched in Ni-bearing Fe sulfides have been interpreted as evidence of water flow in the parent body (Lee et al., 2014; Rubin et al., 2007; Trigo-Rodríguez & Rubin, 2006). Despite the growing documented occurrence of alteration fronts in hydrated carbonaceous chondrites (CO, CM, and C2-ungrouped subtypes), their petrographic features, formation mechanisms, and implications for fluid activity remain poorly resolved. In this study, we investigate alteration fronts in RKP 17085 and compare these features with those previously reported from other carbonaceous chondrites. We provide new insights into fluid migration and aqueous alteration in hydrous primitive asteroids.

MATERIALS AND METHODS

Samples

RKP 17085 is a find recovered from the Reckling Peak ice field, Antarctica (76°12.4917′ S, 158°28.4067′ E), during the 2017–2018 field campaign of the Italian Programma Nazionale delle Ricerche in Antartide (PNRA). This sample was reported in the Meteoritical Bulletin No. 110 as an unshocked (S0), minimally weathered (W1) CM2 chondrite with a total mass of 1.4 g and a magnetic susceptibility (log χ) value of 4.17 (Gattacceca et al., 2022). The petrographic description reports a low abundance of phyllosilicates and the presence of "alteration fronts" dispersed throughout the sample.

We studied two thin sections (RKP 17085-00 and RKP 17085-02), representing a combined surface area of 89 mm^2. Because the two thin sections are similar to each

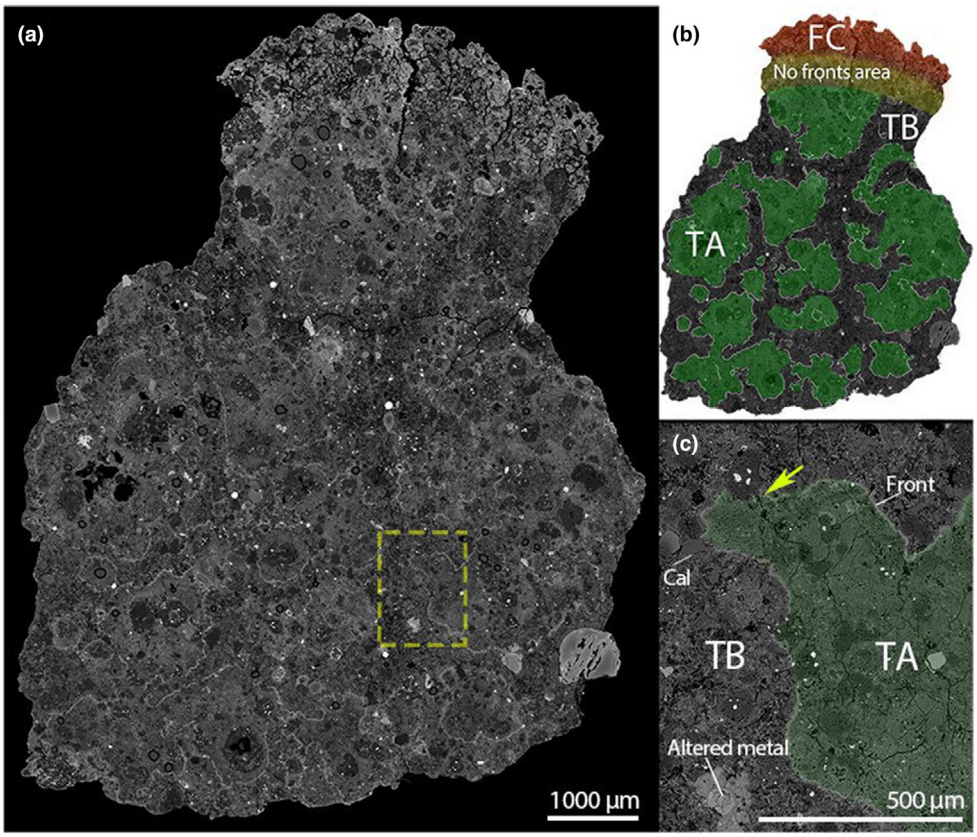

FIGURE 1. (a) BSE image of a thin section (#02) of RKP 17085. (b) Visual representation of the subdivision of the thin section: Type-A (TA) matrix is in green, separated from type-B (TB) matrix by alteration fronts (white lines); the yellow to orange areas define the regions where alteration fronts are not visible and the fusion crust (FC). (c) Zoom-in (BSE) image of the yellow box in (a), with the two types of matrix (TA—in green and TB) separated by the alteration front. Inside the type-B matrix, there is T0 calcite (Cal) and an altered metal blob (surrounded by an Fe-rich aureole). The alteration front is interrupted by a chondrule (yellow arrow).

other, they are collectively discussed in the results section (RKP 17085-02 is taken as reference; Figure 1). Our analysis employed a combination of transmitted and reflected light optical microscopy, scanning electron microscope (SEM), IR spectroscopy and microscopy, and Raman spectroscopy. In addition, a loose chip with a mass of 60 mg was powdered and analyzed using X-ray diffraction (XRD) and thermogravimetric analysis (TGA) to provide bulk mineralogy and volatile abundances, respectively. Finally, a mass of 2 mg was used for bulk O-isotopic analyses.

Bulk Analysis

Modal Mineralogy from XRD

Approximately 50 mg of the powdered meteorite was analyzed by XRD at the Natural History Museum (NHM), London. Initially, we employed a PANalytical X'Pert Pro scanning X-ray diffractometer for high-resolution qualitative mineral identification. A small aliquot of powder (5 mg) was analyzed using monochromatic Co-Kα radiation. Data were collected from 3 to 120° 2θ, with an angular resolution of 0.02° and for approximately 6 h. The resulting pattern was then evaluated against the International Center for Diffraction Data (ICDD) mineral standards library (PDF-2).

For quantitative modal mineralogy analysis, we used an ENRAF Nonius FR 590 X-ray diffractometer fitted with a curved 120° position-sensitive detector (PSD) and monochromatic Cu-Kα_1 radiation, at the NHM, London. Diffraction patterns were collected for 16 h from the meteorite sample and for 30 min from mineral standards. Modal mineralogy was calculated using a profile-stripping method (Cressey & Schofield, 1996), which systematically matches the intensities of relevant diffraction peaks in each mineral standard to the intensity of their equivalent diffraction peaks in the meteorite pattern. The scaled mineral standard patterns were then subtracted from the meteorite pattern, resulting in a residual with (approximately) zero counts. Fit factors for each mineral

standard were corrected against their relative differences in X-ray absorption to produce volume fraction estimates for each phase within the meteorite. The sensitivity of this technique is typically limited to phases with abundances ≥1 vol%, although this depends on the specific phase and the overall mineralogy of the sample. Additional details on the analytical protocol used to determine the modal mineralogy of hydrated carbonaceous chondrites by XRD can be found in Howard et al. (2009, 2015), King et al. (2015, 2019), and others.

Thermogravimetry

Two subsamples of the powder used in the XRD analysis (~11 mg each) were analyzed using a TA Instruments SDT Q600 TGA at the NHM, London. The samples were heated in an inert, flowing N_2 atmosphere at a rate of +10°C min^{-1} from room temperature (18°C) to 1000°C. Volatile emission as a function of temperature is calculated by high-precision measurement of mass change (loss) during heating. Sample mass was measured every 0.5 s using a balance with a sensitivity of 0.1 μg. The overall error on the mass loss fractions is approximately 0.1%. The TGA outputs both a mass-temperature curve and its first derivative (DTG) which reflects the peak temperature of each distinct mass loss event.

TGA is often employed in the analysis of hydrated carbonaceous chondrites (e.g., Garenne et al., 2014) and the approximate temperature ranges of decomposition for the main volatile-bearing mineral groups in carbonaceous chondrites are well established, with adsorbed terrestrial water released at temperatures <200°C, water from Fe-oxyhydroxides released between 200 and 400°C, water from phyllosilicates released between 400 and 770°C, and CO_2 released from the breakdown of carbonates between 770 and 900°C (Garenne et al., 2014; King et al., 2015). The emission of SO_2 gas from the decomposition of Fe and Fe,Ni sulfides (pyrrhotite, troilite, pentlandite, and tochilinite) is often not considered because their volatile release is predicted to be negligible (Fe sulfides composed <4 vol% of the CM mineral assemblage; Howard et al., 2015). However, their decomposition occurs between 400 and 650°C (Burgess et al., 1991; Suttle, Greshake, et al., 2021) and will, therefore, contribute to the "phyllosilicate" emission window. The breakdown of organic matter contributes to mass loss in the same range (Alexander et al., 2007; King et al., 2015).

Oxygen Isotopic Composition

The O-isotopic analysis of an acid-washed aliquot (2.51 mg) was conducted at the Stable Isotopes Laboratory of CEREGE using a laser fluorination system coupled with isotope ratio mass spectrometry (IR-MS; further details of this procedure are given in Alexandre et al., 2006; Suavet et al., 2010).

Petrographic Analysis

Optical images were acquired using a polarizing microscope ZEISS Axioplan equipped with an Axiocam 105 color camera at the Dipartimento di Scienze della Terra of the Università di Pisa and processed with the Axioscope image software. Subsequently, the polished thin sections were coated with carbon (to an approximate thickness of 10 nm) with a high vacuum C-thread evaporator (Leica EM ACE600).

Backscattered electron images (BSE) and energy dispersive X-ray (EDS) spectra (point analyses and maps) were collected at the Centro per l'Integrazione della Strumentazione dell'Università di Pisa (CISUP) using a FEI Quanta 450 field emission gun (FEG) SEM fitted with a Bruker Quantax EDS system and Xflash silicon drift detector, and a dual beam ZEISS Crossbeam 550. Standard-less quantitative EDS analyses were obtained under high vacuum at a fixed working distance of 10 mm with an accelerating voltage of 15 kV and an unmonitored beam current. Weight totals were determined using Bruker's built-in interactive PB/ZAF routine with oxygen directly measured. Geochemical data are quoted as weight-normalized values to one decimal place.

Spectroscopic Analysis

Bulk IR analyses were conducted on a chip (taken away from the fusion crust) at the INAF-Astrophysical Observatory of Arcetri (Italy) with a Bruker VERTEX 70v interferometer interfaced with a Harrick Praying Mantis™ for DRIFTS analysis. During the analysis, the Praying Mantis™ was saturated with a nitrogen atmosphere to rule out any oxidation and contamination due to air. Temperature was constant at about 25°C. The VERTEX 70v was equipped with a DTGLS detector and KBr beamsplitter resulting in a wave number acquisition range from 8000 to 400 cm^{-1} with a spectral resolution of 4 cm^{-1}. Infragold by Labsphere was used as a background reference. Each spectrum was obtained with 100 scans of the interferometer.

IR maps of the alteration fronts and matrix were acquired using a Bruker HYPERION 1000 interfaced with a VERTEX 70v interferometer (as a source of the IR beam). The analyses were conducted on thin section RKP 17085-00 (after the removal of the carbon coat with ethanol). Optical images were acquired using an Infinity 1 camera by Lumenera, while spectra were acquired using an MCT detector. Maps were acquired on different areas to cover the selected region on the thin section. Spectra were acquired in the wave number range from 8000 to

400 cm^{-1} with a spectral resolution of 4 cm^{-1}. The spatial resolution of the IR maps was 50 × 100 μm. Infragold integrated with the Hyperion 1000 sample plate was used for reference, and measurements were obtained in the air at a temperature of about 25°C. Spectra in the map were obtained with a variable number of scans of the interferometer between 100 and 300. Band centers were calculated using local minima/maxima and the peak-picking method on the ORIGIN software (ends points weighted mode).

Raman spectroscopy was conducted at the Dipartimento di Scienze della Terra of the Università di Pisa. Unpolarized micro-Raman analyses were carried out on a polished section in nearly backscattered geometry with a Jobin-Yvon Horiba XploRA Plus apparatus, equipped with a motorized x-y stage and an Olympus BX41 microscope with a 100× objective. The Raman spectra were excited by the 532 nm light of a solid-state laser attenuated to 10%. The system was calibrated using the 520.6 cm^{-1} Raman band of silicon before each experimental session. Spectra were collected through multiple acquisitions (n = 3) with counting times of 30 s. Backscattered radiation was analyzed with a 1200 mm^{-1} grating monochromator.

RESULTS

Modal Mineralogy from XRD

The scanning XRD pattern indicates that the main crystalline phases in RKP 17085 are olivine, pyroxene, magnetite, Fe sulfides, carbonates, and Fe,Ni metal. Diffraction peaks from hydrated phyllosilicates were not detected. We note that the olivine appears to consist of two components; one producing intense, sharp diffraction peaks that we attribute to crystalline, Mg-rich olivine, and the other with much broader reflections from fine-grained and/or poorly crystalline Fe-rich olivine (Figure 2). From the PSD-XRD data (Figure 2a), RKP 17085 contains ~20 vol% olivine, ~15 vol% pyroxene, ~2 vol% magnetite, ~2 vol% Fe sulfides, ~1 vol% carbonate, and <1 vol% Fe,Ni metal. However, following subtraction of the crystalline phases, the residual pattern was still greater than zero counts, indicating the presence in the sample of a highly disordered and/or very fine-grained Fe-bearing phase. Although we cannot rule out some contribution from poorly crystalline Fe-oxyhydroxides and rust (see petrographic description below), we found that the residual was a reasonable match to the shape and intensity (when scaled) of the diffraction patterns of our phyllosilicate standards (excluding the diffraction peaks). We, therefore, attribute the remaining counts in the residual pattern to phyllosilicates (~60 vol%) that were dehydrated during thermal metamorphism and no longer produce coherent diffraction (e.g., King et al., 2015; King, Schofield, & Russell, 2021; Nakamura, 2005).

Volatile Abundance from TGA

RKP 17085 experienced a 19.1 wt% mass loss as it was heated over the temperature range of 20–1000°C (Figure 3, Figure S1, Table S1). A significant fraction of the mass loss (8.9 wt%, ~50%) occurred at low temperatures (<200°C). Mass loss over this range is conventionally attributed to the emission of adsorbed terrestrial water and the breakdown of weathering products such as sulfates (e.g., Garenne et al., 2014; King et al., 2015). At higher temperatures, RKP 17085 lost 3.7 wt% over the 200–400°C range (attributed to Fe-oxyhydroxide phases), 5.7 wt% between 400 and 770°C (attributed to SO_2 emission from sulfides, $H_2O/CO_2/SO_2$ from IOM and OH emission from phyllosilicates), and 0.7 wt% from 770 to 900°C (attributed to CO_2 emission from carbonates) (Figure 3). Based on the methods of Garenne et al. (2014) and King et al. (2015), the estimated H_2O content (mass loss from 200 to 770°C) of RKP 17085 is ~9.4 wt%.

Bulk Oxygen Isotopes

The oxygen isotopic composition of RKP 17085, from analysis of a single, acid-washed bulk sample, is $\delta^{17}O = -5.052‰$, $\delta^{18}O = -3.153‰$, $\Delta^{17}O = -3.412‰$ (slope 0.52, analytical uncertainties of 0.115‰, 0.062‰, 0.005‰ for $\delta^{17}O$, $\delta^{18}O$, and $\Delta^{17}O$, respectively). In $\delta^{17}O$-$\delta^{18}O$ isotope space RKP 17085 plots away from the main CM group ($\delta^{17}O = -3.87$ to 11.59‰, $\delta^{18}O = -1.23$ to 22.29‰, $\Delta^{17}O = -4.16$ to 0.30‰, Clayton & Mayeda, 1999) and is, instead, closer to the isotopic composition of the CO group ($\delta^{17}O = -6.72$ to −3.13‰, $\delta^{18}O = -4.33$ to 1.21‰, $\Delta^{17}O = -4.72$ to −3.76‰; Clayton & Mayeda, 1999). This position is similar to that of the recently reported minimally aqueously altered (CM ≥2.7) "Asuka CMs" (A-12085, A-12169, and A-12236, ranging from $\delta^{17}O = -5.98$ to 3.29‰, $\delta^{18}O = -2.07$ to 10.82‰, and $\Delta^{17}O = -4.90$ to −2.34‰; Kimura et al., 2020; Figure 4; Table S2).

Petrography

RKP 17085 contains chondrules (few readily delineated) with a mean diameter of 220 ± 140 μm (1σ) (N = 72; intact chondrules only). Calcium–Aluminum-rich inclusions (CAIs) are rare (<1 area%). Refractory inclusions are set into a dark-opaque fine-grained matrix. Chondrule abundance is ~25 area%, matrix abundance is ~70 area%, and opaque mineral abundance is <2 area% (of which metal is ~0.4 area%).

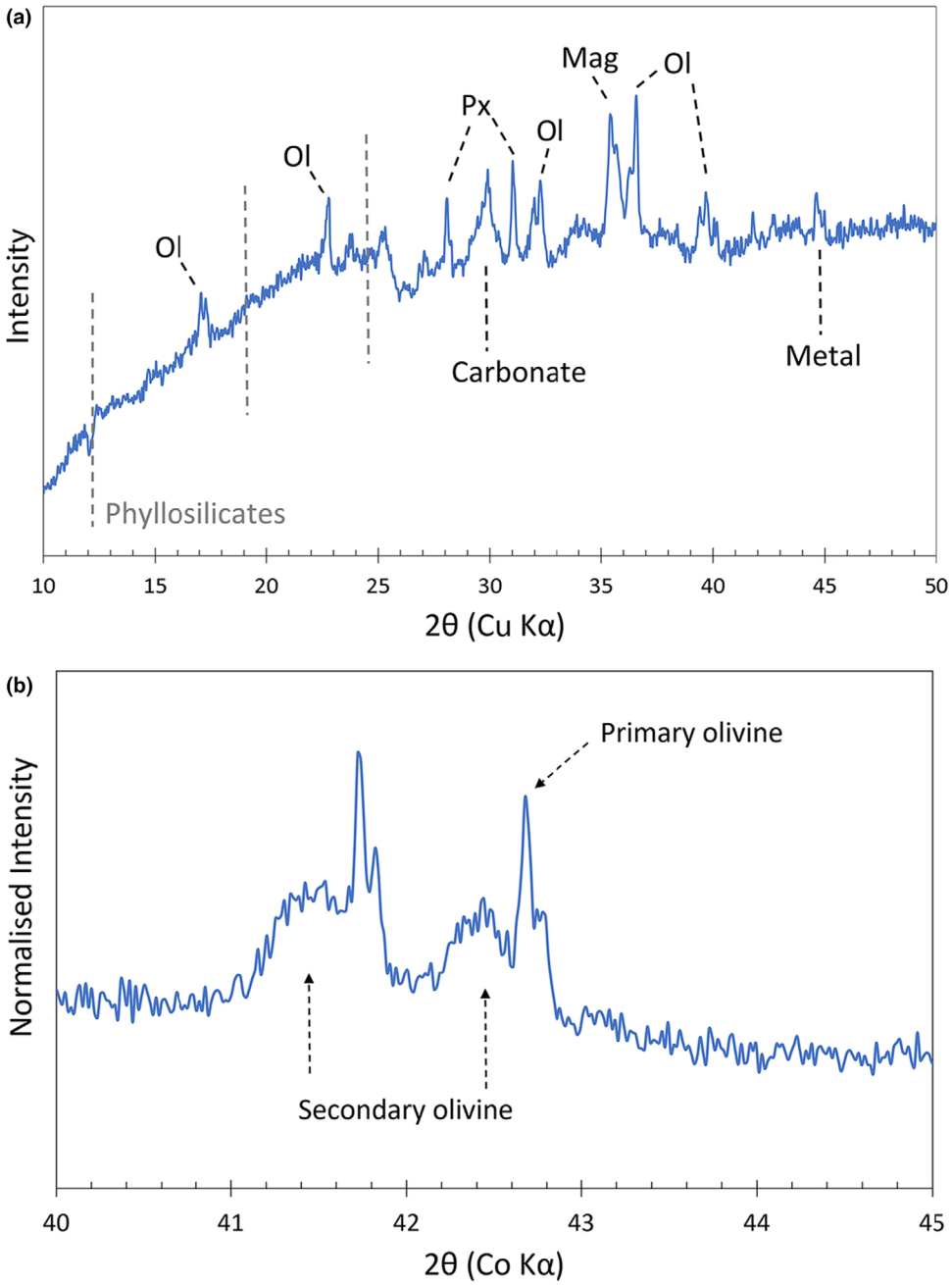

FIGURE 2. (a) PSD-XRD pattern for RKP 17085 with the main diffraction peaks labeled. Ol, olivine; Px, pyroxene; Mag, magnetite. Diffraction peaks associated with phyllosilicates in CM chondrites (positions indicated by the gray dashed lines) were not observed in RKP 17085. (b) Scanning XRD pattern highlighting the presence of crystalline primary (sharp peak), and poorly crystalline secondary (broad peak) olivine in RKP 17085.

Fine-Grained Matrix and Alteration Fronts

RKP 17085 has a bimodal appearance with two distinct types of matrices separated by a complex network structure (white traces in Figure 1b). We term these regions type-A and type-B matrix, and the network structure as "alteration fronts". Excluding the fusion-crusted margin, which occurs along one side of the studied sections, type-A matrix composes approximately 55 area% of the sample and is characterized by a compact, low porosity (~7%), fine-grained texture, and homogeneous Z-contrast in BSE images. Conversely, type-B matrix (45 area%) has a higher porosity (~15%), as evidenced from BSE images and fewer dehydration cracks. Both type-A and type-B matrices have

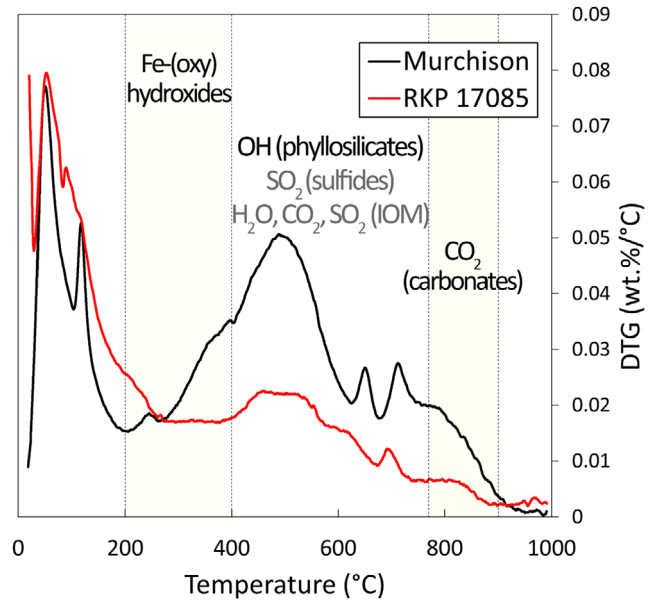

FIGURE 3. DTG curves for the CM chondrites RKP 17085 (red; aliquot "a" in Table S1) and Murchison (black). The limited rate of change (and, then, mass loss) of RKP 17085 over the range of 400–770°C is evidence of the minor content of hydrated phyllosilicates when compared to Murchison. For RKP 17085, the mass loss over the range of 400–770°C can mainly be due to the decomposition of sulfides and IOM. The minor content of hydrated phyllosilicates in RKP 17085 is explained by post-hydration metamorphism (as documented in other heated CM/C2; Garenne et al., 2014), and in agreement with morphological features like subparallel cracks in the fine-grained rims.

the same approximate bulk chemical composition (in wt%: Fe = 31.2, Si = 15.4, Mg = 8.7, S = 1.6, Ni = 1.8; Figure 5). Type-B matrix is characterized by homogeneously distributed, irregular void space 3 μm across (average Feret size of pores in an area of 1.2 mm^2).

The boundaries between the two different matrix textures are well defined and outlined by 10- to 40-μm-thick layers with a compact structure, sinuous profiles, and lobate-cuspate geometry: the alteration fronts (Figure 6a,b). In thin sections, the alteration fronts show up as thin ribbons of dark-brown color, when observed in transmitted light, or bright gray with high *Z*-contrast, when observed in reflected light in the optical microscope or BSE imaging in the SEM. They have an Fe-rich chemical composition (i.e., in wt%: Fe = 38.8, Si = 10.8, Mg = 6.0, S = 1.5, Ni = 1.4, Cl <0.2), and so they represent, on average, local enrichments in Fe (+8 wt%; Figure S2) compared to the fine-grained matrix. Based on the BSE imaging and EDS compositions, the alteration fronts are interpreted as extremely fine-grained Fe-oxyhydroxide minerals such as goethite ($[Fe^{3+}]O[OH]$) or ferrihydrite (e.g., $[Fe^{3+}]_2O_3{\cdot}0.5H_2O$) intermixed with the fine-grained matrix.

Finally, an additional bright phase (high Z-contrast in BSE), with an acicular habit and radiating morphology (termed the "needle-like" phase; Figure 6b,c) is found throughout the meteorite, occurring in both the type-A and type-B matrix. These needle-like crystals are Fe-rich (52.2 wt%) and contain O (35.1 wt%), Si (3.6 wt%), Mg (3.0 wt%), S (2.5 wt%), and Ni (1.8 wt%), as major elements (Figure 5; Table S3). The content of Cl is 0.1–0.8 wt%. They are also interpreted as a hydrated ferric oxyhydroxide mineral (goethite and/or ferrihydrite). We note that the needle-like phase crosscuts the alteration fronts (Figure 6c).

Chondrules, CAIs, and Isolated Anhydrous Silicates

Chondrules are exclusively porphyritic and granular subtypes belonging to the compositional type IA or A/B (FeO-poor). Olivine (pure forsterite) and pyroxene ($En_{99.7\pm0.7}$, $Wo_{0.4\pm0.7}$, $N = 7$) are their main phases, while metal (kamacite, taenite), Fe sulfides (pyrrhotite, troilite), and altered mesostasis (in wt%: Fe 33.9, Si 13.6, Mg 9.4, Al 3.3; S 1.3 [$N = 2$]; Figure S3, Table S3) occur as minor phases.

Anhydrous silicates are also widespread within the fine-grained matrix where they occur as isolated mineral fragments with sizes up to 500 μm and subangular morphologies. Several of these are severely fractured and typically have more Fe-rich (fayalitic) compositions, relative to the chondrule silicates; average olivine values are $Fa_{30\pm22}$ ($N = 29$) and low-Ca pyroxenes are $Fs_{9\pm22}$ ($N = 7$). High-Ca pyroxene crystals are relatively rare, but when present occur as diopside ($Fs_{3\pm4}$, $Wo_{50\pm6}$, $N = 2$; Tables S4 and S5). Both chondrules and mineral fragments are surrounded by fine-grained rims (FGR), which contain numerous radial cracks that crosscut the entire rim.

Only two small refractory inclusions (CAIs) were identified. One has a fine-grained texture, with a Ca-rich core surrounded by an Al-rich rim. The other CAI is composed of spinel (V-bearing $MgAl_2O_4$) with perovskite inclusions ($CaTiO_3$) and is associated with Ni-bearing troilite.

Opaque Phases

Opaque phases include metal, magnetite, and Fe sulfides. Metal grains are primarily kamacite (Ni 4.1–6.5 wt%) and occur as equant, rounded objects, predominantly within chondrules, with sizes up to 100 μm diameter. These grains have well-defined boundaries and minimal evidence of physical–chemical alteration (Figure S4a). Metal is also present as smaller irregular-shaped grains dispersed within the matrix. Magnetite occurs within the matrix as small (<10 μm) rounded and

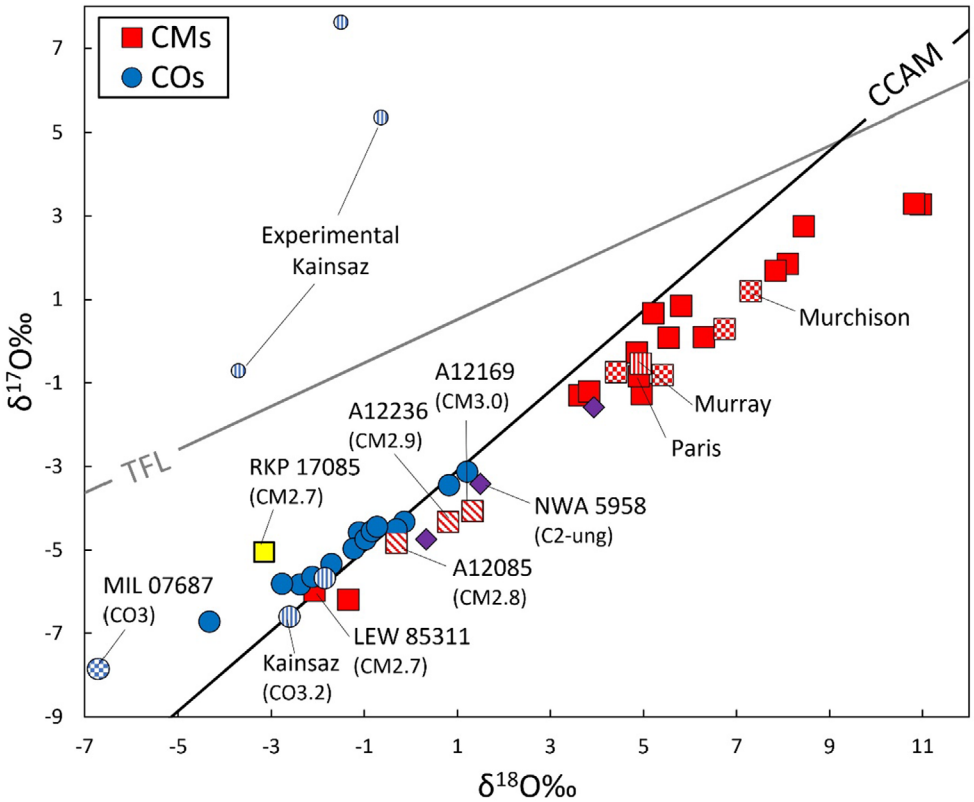

FIGURE 4. Bulk O-isotopic composition of RKP 17085 compared to CM (Greenwood et al., 2023, and references therein) and CO (Clayton & Mayeda, 1999) chondrites including those reported to have alteration fronts (e.g., Murchison, Murray, MIL07687, and the C2-ung NWA 5958) (Jacquet et al., 2016; Prestgard et al., 2021). RKP 17085 (yellow square) has a similar $\delta^{18}O$ composition to the CM2.7 chondrite LEW 85311 (Lee et al., 2019), but has a higher $\delta^{17}O$ value that seems to follow the variation trend of the experimentally altered samples of the CO3.2 Kainsaz (doped with heavy water, Suttle et al., 2022). All data are given in Table S2.

equant grains. They contain Ni (1.5–3.0 wt%) and have trace quantities of Na (<0.6 wt%), Mg (<0.7 wt%) and Mn (<0.4 wt%). Plaquette and framboidal morphologies were not observed.

Iron sulfides are common as irregular-shaped grains found intergrown with phyllosilicates or as larger grain clusters surrounding chondrules and isolated anhydrous silicates. Pyrrhotite-troilite group minerals are overwhelmingly the dominant sulfides and include both high-Ni (20–34 wt%) compositions (present within chondrules) and low-Ni (<0.5 wt%) (within the matrix). The at% Fe/S ratios of low-Ni sulfides approach values of 1.0, reflecting troilite endmember compositions. We also detected rare pentlandite and a single grain of daubréelite ($[Fe^{2+}][Cr^{3+}]_2S_4$). However, tochilinite and associated TCIs, common components of CM chondrite mineral assemblages, were not detected.

Carbonates

Carbonates are a relatively minor phase in RKP 17085. They occur as irregular-shaped subhedral grains lacking inclusions or voids and are tens of micrometers in size. The carbonates do not have overgrowth rims and their grain margins reveal evidence of etching (Figure S4b). Carbonates are single-phase calcite (identified using Raman spectroscopy; Figure S5) and have relatively pure compositions with low amounts of Mg (<0.7 wt%), Fe (<1.5 wt%), and Mn (<0.5 wt%). Carbonates in RKP 17085 are interpreted as exclusively type 0 (hereafter: T0) calcites (i.e., calcite with neither rims nor inclusions; Vacher et al., 2017). Rimmed or inclusion-bearing "T1" calcites and polycrystalline "T2" calcites (associated with later events of precipitation; Lee et al., 2014), which are otherwise common in CM chondrites (Vacher et al., 2017) are not present in this sample.

Fusion Crust

Fusion crust is present along one margin of the meteorite. It is highly fractured and vesiculated with a microphyritic quench texture. It is composed of crystallites of olivine and microdendrites of Fe-oxides set in a glassy matrix. It contains relict anhydrous minerals

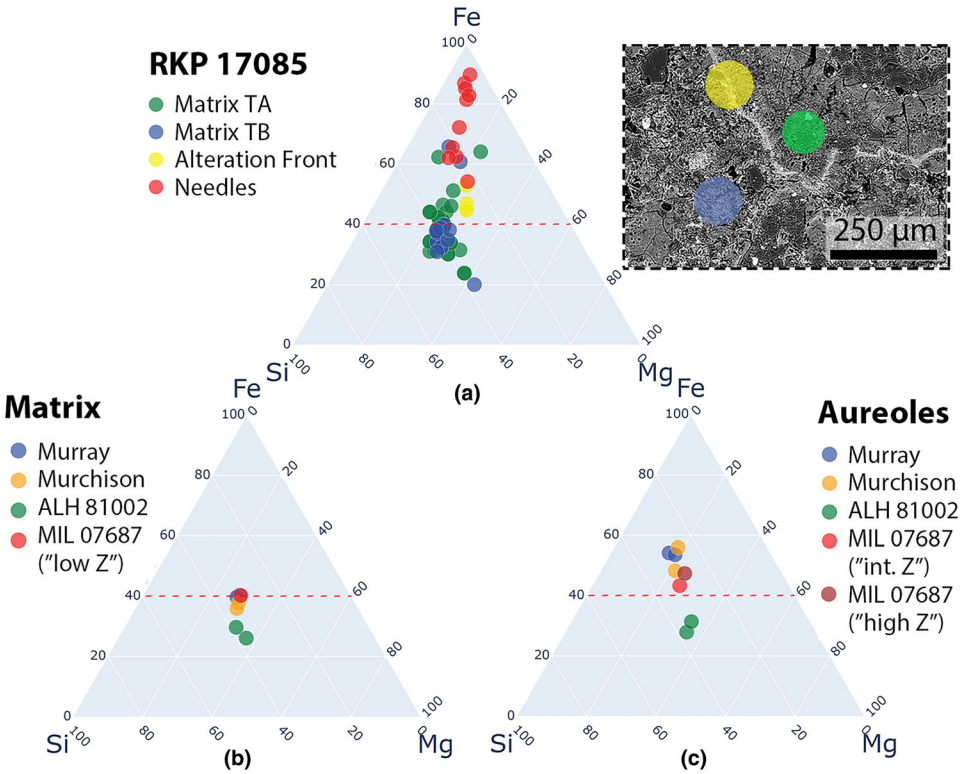

FIGURE 5. Ternary plots with Fe-Si-Mg (atom%) of (a) RKP 17085, for its different components (matrix TA, matrix TB, alteration fronts, needles—on the right, a BSE image as a reference); (b) matrix in the CM2 chondrites Murray, Murchison, and ALH(A) 81002 (Hanowski & Brearley, 2000), and CO3 MIL 07687 (considering the low-Z matrix described in Haenecour et al., 2020); (c) aureoles in the same chondrites, for MIL 07687 are considered the phases indicated as "Intermediate Z" and "High Z" (Haenecour et al., 2020).

(predominately olivine) with embayed textures. Fractures within the fusion crust are lined with layered deposits of goethite, and some regions close to the fusion crust are also infilled by goethite. The network of alteration fronts cannot be traced toward the fusion crust (top of Figure 1b). The branches of the fronts closest to the fusion crusts are not connected to the layered deposits of goethite in veins. Instead, the needle-like phase, which is observed together with alteration fronts and in type-B matrix, is present also in proximity to the fusion crust (Figure 6d).

IR Spectroscopy

Figure 7 compares the near- and mid-infrared (NIR and MIR) bulk reflectance spectrum of RKP 17085 to those of the CM2 chondrites, Murchison, ALH(A) 81002, Murray, and the CO3 chondrite MIL 07687. These are chondrites that also have reports of fronts/aureoles but are classified with different degrees of aqueous alteration (Table 1). The spectra of a primitive CO3, Dominion Range (DOM) 08006, and of the CM2 Yamato (Y)-86695 are used as a benchmark for a more representative CO and a thermally metamorphosed CM chondrite spectra, respectively. We observe that:

- The 3-µm band (OH/H_2O) of RKP 17085 is centered at 2.80 µm. The wide shape of RKP 17085's 3-µm band is indicative of a high content of adsorbed water in the sample, in agreement with the TGA results.
- The position of the Christiansen feature (CF), which is at 8.5 µm for RKP 17085, has previously been shown to change with the degree of alteration (Bates et al., 2020; Hanna et al., 2020; McAdam et al., 2015), moving to longer wavelengths for more altered chondrites (toward 9 µm in Figure 7b).
- RKP 17085 lacks a strong "W-shape" feature over the wavelength range of 13–25 µm. The absence of this feature is consistent with less aqueously altered CM chondrites (McAdam et al., 2015).
- In all spectra, RKP 17085 and Murchison are broadly similar but RKP 17085 has a stronger signal for anhydrous silicates (forsterite and enstatite, with features between 9 and 10 µm; Figure 7b,c). Murray, ALH(A) 81002, and MIL 07687 spectral features significantly differ from that of RKP 17085 (especially in the range 8–18 µm; Figure 7b).

In addition, we used MIR spectroscopy to assess the variation of the spectra on the fronts and

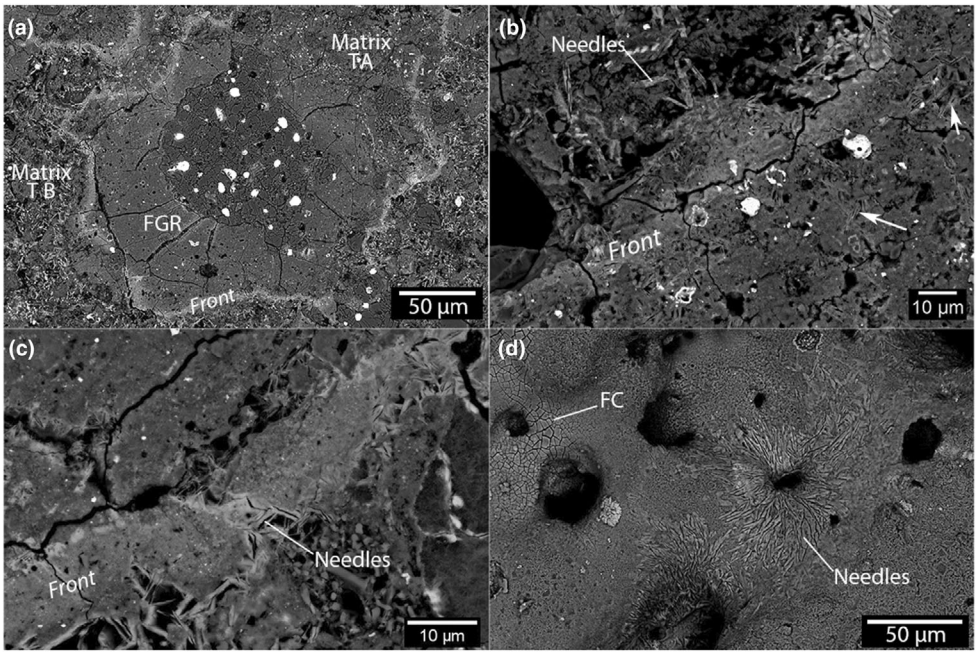

FIGURE 6. BSE images of RKP 17085. (a) Alteration front surrounds a type I chondrule with a fine-grained rim (FGR) with dehydration cracks. The matrix type-B (more porous) is outside the area surrounded by the alteration front. (b) The alteration front and needles are in close relation, clearly in the upper part of the front and in the matrix below (white arrows). (c) Needles in crosscutting relation with alteration front. (d) Image acquired on the external, fusion-crusted surface of RKP 17085 showing Fe-oxyhydroxide needles overgrowing the fusion crust (FC) and filling the walls of degassing pipes.

the surrounding matrix and identify the mineralogy in the needles. Matrix spectra are very similar across the entire meteorite and show no difference when compared with the spectra of the fronts (Figure S6a,b,d). Matrix spectra show a strong Si-O stretching band at 10 µm and the OH absorbance band at 2.75 µm similar to the ones observed by Dionnet et al. (2018) and Noun et al. (2019) in the mildly altered CM chondrite Paris, and interpreted as hydrated amorphous silicate (Figure S6b). Needles do not show distinct features, likely due to the dominant signal from the matrix and limited spatial resolution. However, goethite and the presence of other Fe-oxyhydroxides have been detected in two cases (Figure S6c).

Raman Spectroscopy

Raman spot analyses within the fine-grained matrix produce characteristic D- and G-bands arising due to the excitation of disordered macromolecular carbonaceous material. In RKP 17085, Raman spectra produce profiles with shallow, broad D-bands and sharper, more intense G-bands (Figure S7). Type-A and type-B matrices do not produce statistically different Raman profiles suggesting that there is no relationship between macromolecular carbonaceous matter and alteration style in RKP 17085.

DISCUSSION

Fe-Oxyhydroxides, Discriminating Parent Body Aqueous Alteration from Terrestrial Weathering

The most unusual aspect of RKP 17085 is the pervasive presence of alteration fronts spread abundantly across the sample (Figure 1). These closely resemble in texture (morphology and relation to other components), thickness (10–40 µm), and composition (enriched in Fe) those described by Hanowski and Brearley (2000) in three CM chondrites (Murray, Murchison, and ALH[A] 81002) and those described in two other hydrated carbonaceous chondrites: the CO3 MIL 07687 (Brearley, 2012; Haenecour et al., 2020; Prestgard et al., 2021) and the C2-ungrouped meteorite NWA 5958 (Jacquet et al., 2016) (Table 1). Alteration fronts in these chondrites act as boundaries, separating a zone of Fe-rich matrix behind the front from a zone of Fe-poor matrix ahead of the front. Sometimes the Fe-rich matrix has a roughly circular shape and is formed around a central altered object; this led to the use of the term "aureoles" by Hanowski and Brearley (2000).

The fine-grained matrix and alteration fronts in RKP 17085 (Figure 5) are comparable in terms of major element chemistry to those reported from the other five "front-bearing" chondrites (Murray, Murchison, ALH[A]

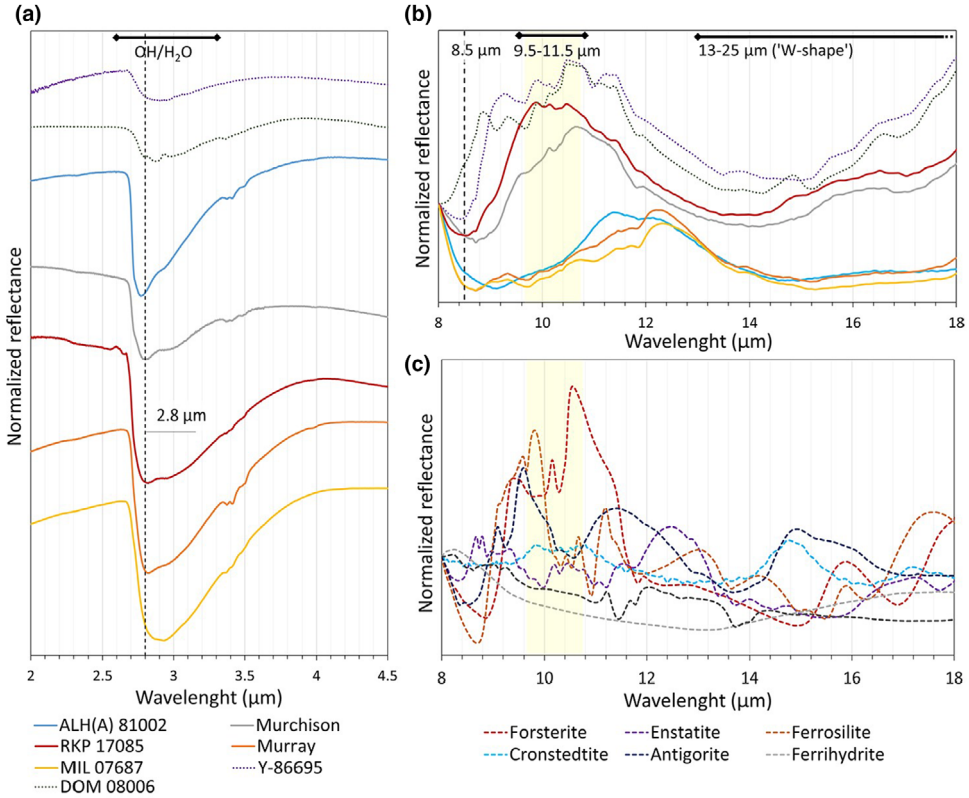

FIGURE 7. Near- and mid-IR spectra of RKP 17085 (red), Murchison (gray), ALH(A) 81002 (blue), Murray (orange), MIL 07687 (yellow), the CO3.0 DOM 08006 (gray dotted), and the thermally metamorphosed CM2 Y-86695 (purple dotted). (a) The 3-µm band center of RKP 17085 is at 2.80 µm, intermediate between MIL 07687 (2.93) and ALH(A) 81002 (2.77). In comparison to the CM (or CM-like) chondrites, DOM 08006 has a shallower band. The spectra are normalized to unity at 2.3 µm and offset for comparison. (b) Mid-IR spectra in the range 8–18 µm: RKP 17085's CF is at lower wavelengths (8.5 µm) compared to the other chondrites (except for Y-86695 and DOM 08006); the Si-O stretching band is sharp and with more overlapping bands as previously reported for other Stage III CM chondrites (Hanna et al., 2020). The spectra are normalized at 8 µm. (c) Spectra at the same wavelengths as (b) of mineral analogs for RKP 17085. The spectra are normalized at 8 µm. The spectra of Murchison, ALH(A) 81002, Murray, MIL 07687, DOM 08006, and Y-86695 are from the RELAB database (MB-TXH-064-C, MB-TXH-050, MT-JMS-189, MT-KTH-284, MP-TXH-271, and MP-TXH-158, respectively), as are those of forsterite (JB-JLB-945-D), enstatite (DD-MDD-167), antigorite (AT-TXH-002), ferrihydrite (JB-CMP-046-A), and goethite (JB-JLB-H57). Cronstedtite is from the RRUFF database (R061026).

81002, MIL 07687, and NWA 5958, although Murray has somewhat lower Fe contents overall). Although chemically similar, petrographically the alteration fronts in RKP 17085 are distinct. Crucially, on either side of the alteration fronts, the fine-grained matrix has a similar chemical composition (Figure 5a) and there is no discernible difference in the degree of alteration. Based on the chemical data (from EDS analysis) and IR spectroscopic signatures the alteration fronts are interpreted as regions of fine-grained matrix that contain an additional, poorly crystalline Fe-rich, O-rich phase. Thus, the alteration fronts in RKP 17085 appear to be zones of local Fe and Ni enrichment, present as fine-grained Fe-oxyhydroxides.

RKP 17085 contains an additional Fe-oxyhydroxide phase, with a similar composition but a distinct texture. The needle-like phase occurs as small (<20 µm), acicular grains often with radiating morphologies (Figure S4c). Similar flaky Fe-oxyhydroxide phases, in terms of texture and composition, were described by Haenecour et al. (2020) within the CO3 chondrite MIL 07687. They were identified as ferrihydrite and interpreted as parent body in origin. However, MIL 07687 was subject to more advanced terrestrial weathering (classified as "CE" in The Meteoritical Bulletin, 2023–reflecting severe rust and the presence of evaporative encrustation) relative to RKP 17085. Because Fe-oxyhydroxide minerals (goethite and ferrihydrite) can be formed either during aqueous alteration or terrestrial weathering, it is difficult to discriminate their origin, especially in meteorites which have remained on the Earth's surface for long and unquantified periods of time and are recovered as "finds" (e.g., RKP 17085 and MIL 07687). In RKP 17085, we interpret the flaky oxyhydroxide needle-like phase as a product of terrestrial weathering,

formed while the meteorite resided in Antarctica, conversely, the more abundant and pervasive alteration fronts are interpreted as features formed during parent body aqueous alteration. Nevertheless, the terrestrial origin of the needle-like phase in RKP 17085 does not exclude the possibility that these phases can originate in the parent body for other chondrites. In support of this idea is the apparent rarity of Fe-oxyhydroxide needles in other Antarctic carbonaceous chondrites (e.g., Renazzo-type CR chondrites, which have a significant amount of metal; Abreu & Brearley, 2010).

The interpretation regarding RKP 17085 is based on the following arguments:

- *Fe-oxyhydroxide crosscutting relationships*: The needle-like phases crosscut the alteration fronts (Figure 6c) allowing a relative chronology to be inferred with the needle-like phase postdating the alteration fronts.
- *Features relative to the fusion crust*: The fusion crust provides a single event in the meteorite's history whose formation location (Earth) and approximate timing (geologically recent) are known. Cracks within the fusion crust contain minor weathering rim encrustations (Figure S4f). This is evidence that limited terrestrial weathering affected RKP 17085. Critically, the needle-like phases are found as overgrowths on the fusion-crusted meteorite exterior, infilling degassing pipes and fractures perpendicular to the sample (Figure 4d). Because Fe-oxyhydroxides are heat-sensitive and thermally decompose at temperatures <400°C (Garenne et al., 2014), the presence of these needle-like phases near the fusion crust requires that they formed after the fusion crust, as a result of weathering. By contrast, the alteration fronts cannot be found close to the fusion crust, preventing a clear crosscutting relationship but implying that any alteration fronts near the fusion crust were destroyed during heating and, therefore, that the alteration fronts pre-date atmospheric entry.
- *The presence of chlorine*: The presence of Cl at low abundances (<1.0 wt%) in Fe-oxyhydroxide minerals is a characteristic feature of extraterrestrial materials affected by Antarctic weathering; in this region, sea spray acts as the source of Cl (Van Ginneken et al., 2016). In RKP 17085, we detected Cl in the needle-like phases (0.1–0.8 wt%), while Cl was absent or close to the detection limit (<0.2 wt%) in the alteration fronts.
- *Relationship between alteration fronts and chondrules*: In most instances, the alteration fronts enclose areas containing chondrules (Figure 6a). A possible explanation for their formation is a fluid movement going outwards from multiple discrete point sources in the matrix TB. On the other hand, terrestrial weathering is expected to migrate from the external surface inwards along fractures, and thus form veins (Figure S4e,f). It is not pervasive and does not cut through all the meteorite components, rather it is generally confined toward the external surface of the meteorite. Aqueous alteration, as delineated by the alteration fronts, is pervasive, shows no relationship with distance from the external surface, and affects mainly the matrix (and not more compact/resistant components like chondrules and their FGRs).
- *The absence of alteration fronts in weathered COs*: We note that the alteration fronts found in RKP 17085 and the other five carbonaceous chondrites are relatively rare features, not otherwise found in the numerous weathered Antarctic CO or CM chondrites. Thus, it is unlikely that weathering produces the alteration front features.

Similar alteration fronts were reproduced in short-term (175 days) hydrothermal experiments using the CO3 chondrite Kainsaz (Suttle et al., 2022), with a water/rock ratio of 0.4, at temperatures of 50 and 150°C. The fronts reproduced are fine grained and enriched in Fe and S. Here, the origin of the fronts was due to the short-lived fluid presence arising due to open system water loss. It is possible that the fluid episodes on RKP 17085 could have been similarly short and that fluids were either consumed completely or escaped due to impact or sublimation. In the fronts of RKP 17085, as for the experiments in Suttle et al. (2022), the formation of Fe-oxyhydroxides in the place of the Fe^{3+}-rich serpentine cronstedtite (as would normally be expected) and the absence of tochilinite are both indications of the conditions in which the metal alteration occurred: oxidizing environment and in presence of low activity of Si^{2+} and S (Suttle, Daly, et al., 2023). Differently from the reducing conditions that are normally attributed to aqueously altered CM chondrites, in which cronstedtite and tochilinite would form (Peng et al., 2009; Peng & Jing, 2014; Vacher, Truche, et al., 2019).

Parent Body History of RKP 17085

RKP 17085 records a complex parent body alteration history characterized by aqueous alteration that appears to have been partially overprinted by thermal metamorphism, as evidenced by the presence of dehydrated phyllosilicates (see Thermal Metamorphism section below). This is consistent with the alteration sequence of the CM chondrite group, in which the entire population was (variably) affected by aqueous alteration (e.g., King, Mason, et al., 2021; Suttle, King, et al., 2021) and approximately a third of the CM chondrites show evidence of post-hydration thermal metamorphism (e.g.,

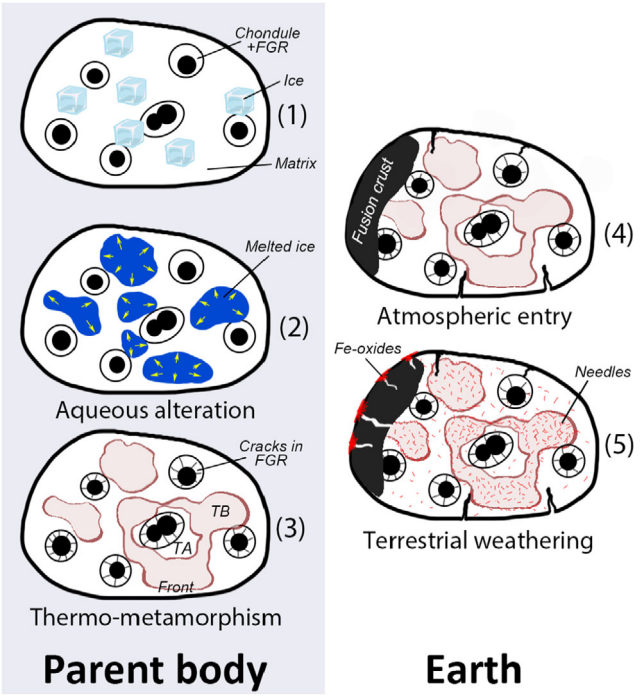

FIGURE 8. Schematical representation of the alteration history of RKP 17085: (1) the parent body is unaltered and contains primordial ice grains inside the matrix; (2) a trigger (e.g., radionuclide decade, shock heating) causes the melting of the ice (centrifugal propagation from the source) and the aqueous alteration that is homogenously distributed (at the scale of the meteorite) but not affecting all the mass; (3) an abrupt change in temperature conditions (<750°C) causes the propagation of water to stop, leaving behind a more porous matrix (type-B, brown areas) and an Fe-rich front where the mobilized Fe^{2+} precipitated, and rapid dehydration causes cracks on the fine-grained rims around chondrules; (4) a collision on the parent body frees part of the asteroid mass, a fragment crosses the Earth's atmosphere forming a fusion crust that partially erases (due to the heating) alteration fronts in its proximity; (5) the meteorite is affected by terrestrial weathering during its residence in the Antarctic ice, mainly forming needle-shaped Fe-oxyhydroxides that preferentially crystallize in the porous type-B matrix and the fusion crust. The size of the components represented is not to scale (see text for a detailed description).

King, Schofield, & Russell, 2021; Krietsch et al., 2021). Figure 8 summarizes each of the processes recorded in RKP 17085.

Aqueous Alteration Extent

The extent of aqueous alteration can be estimated from the modal mineralogy using the scheme of Howard et al. (2015), which is based on the phyllosilicate fraction (PSF: Total phyllosilicate/[total anhydrous silicate + total phyllosilicate] by volume) as a metric for the progression of aqueous alteration. Despite the overprinting effects of

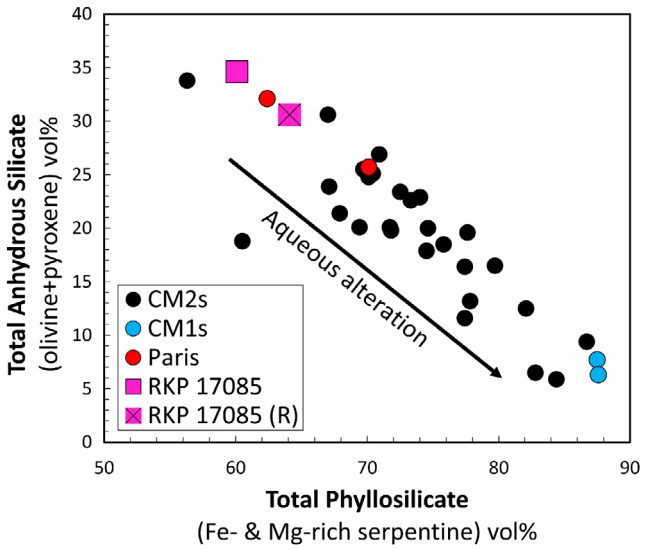

FIGURE 9. Total abundance of phyllosilicates and anhydrous silicates (CM2s and CM1s data are from Howard et al., 2015 and King, Mason, et al., 2021; Paris data are from Krietsch et al., 2021). For RKP 17085, besides the abundance directly analyzed (simple square symbol), it is also plotted the reconstructed (R) mineralogical composition prior to thermal metamorphism and recrystallization (barred square; see Aqueous Alteration Extent section).

thermal metamorphism, the amount of former phyllosilicate can be inferred from the combined abundance of secondary olivine (~4 vol%, formed by recrystallization of dehydrated phyllosilicates and identified here by the broad olivine diffraction peaks in XRD; see Thermal Metamorphism section) and poorly crystalline phyllosilicates (~60 vol%; Suttle, Greshake, et al., 2021). Our reconstructed PSF for RKP 17085 is 0.68 (Figure 9). This translates to a petrologic subtype of 1.7 on the scale of Howard et al. (2015), equivalent to a CM2.6 on the Rubin scale (Rubin et al., 2007), and indicates a mild degree of aqueous alteration. However, the absence of TCIs is not consistent with a 2.6 subtype as described by Rubin et al. (2007), and is perhaps in better agreement with a CM2.7/2.8 classification following Kimura et al. (2020). A subtype of 2.7 is suggested for RKP 17085, based on the following features:

- RKP 17085 lacks TCIs, or their dehydration products (Fe-S-O clumps containing magnetite and amorphous Mg-Fe silicates, e.g., Lee et al., 2016). These are a relatively major component of the CM chondrite lithology and common in CMs with an alteration extent between CM2.6 and CM2.2 (Rubin et al., 2007; Suttle, Daly, et al., 2023) but are absent from the Asuka CMs (CM2.8-3.0; Kimura et al., 2020).
- In CM chondrites, kamacite is one of the earliest phases to be attacked by fluids and dissolved (Palmer

& Lauretta, 2011; Pignatelli et al., 2017; Rubin et al., 2007). Indeed, according to Rubin et al. (2007), a metal content of 1 vol% (petrographic estimation) is indicative of a minimum subtype of 2.6. RKP 17085 retains large (>50 μm) unaltered metal grains (Figure S4a) suggesting that it was altered under a fluid-limited regime (low water-to-rock [W/R] ratios) and, therefore, the duration of aqueous alteration was likely short lived. This is in agreement with the magnetic susceptibility (log χ) value of RKP 17085 (4.17), compatible with CM chondrites (that can vary from 3.19 to 4.94, Rochette et al., 2008).

- On the CM parent body, multiple generations of carbonate were precipitated during aqueous alteration dependent on the fluid composition, pH, and temperature (Lee et al., 2014; Lindgren et al., 2017). At least three generations (T0, T1, and T2) of calcite with distinct morphologies and petrographic settings are recognized (Vacher et al., 2017; Vacher, Piralla, et al., 2019). Often, a single CM meteorite preserves more than one calcite generation, reflecting the progression of aqueous alteration and preservation of earlier-formed generations. However, in RKP 17085, only the T0 calcites (irregular-shaped subhedral grains which lack inclusions or voids) are found. Through petrographic observations, Vacher, Piralla, et al. (2019), Vacher, Truche, et al. (2019) state that T0 calcites postdate type-1a Ca-carbonates. The presence of only T0 calcite can be a result of different physicochemical conditions for the alteration of RKP 17085 (e.g., outside the stability of tochilinite, which constitutes, with cronstedtite, the rims in type-1a carbonates).
- The 3-μm near-IR absorption band center of RKP 17085 is located at 2.80 μm. This position usually reflects a higher abundance of Fe-rich serpentines (vs. Mg-serpentines). For RKP 17085, since the phyllosilicates are partially dehydrated, it likely reflects the presence of Fe-oxyhydroxides (e.g., ferrihydrite, see Figure 11 in Pommerol et al., 2009). In more aqueously altered CM chondrites, Mg-rich serpentines usually begin to dominate spectrally, causing a shift in the 3 μm feature to shorter wavelengths with petrologic types of 1.5 or less (in the scheme of Bates et al., 2020; Howard et al., 2015; Takir et al., 2013, 2019). At longer, mid-IR wavelengths (~8–20 μm), a poorly resolved "W" shape feature is also indicative of a low degree of aqueous alteration (McAdam et al., 2015; Takir et al., 2013, 2019). Usually, as aqueous alteration proceeds and Mg-rich serpentines increase in abundance, a feature at 16 μm caused by Mg-OH becomes more distinguishable, causing a more prominent "W" shape to appear in the most altered samples (Hanna et al., 2020; McAdam et al., 2015). The absence of this feature in mid-IR spectra of RKP 17085 is consistent with it having experienced only mild aqueous alteration. It is important to consider that thermal alteration also affects the spectra, eventually erasing traces of pre-heating aqueous alteration. For chondrites at Stages ≥III (500–750°C, in the Nakamura, 2005 classification scheme), the Si-O stretching band (9–12 μm) has a sharper profile, with more overlapping bands compared to samples subjected to lower heating, while the 3-μm band center moves to longer wavelengths and evolves to a broader, and more symmetric shape (Hanna et al., 2020). Thus, the spectra of RKP 17085 are in good agreement with Stages III and IV (>750°C) heated CM chondrites.

Consequently, RKP 17085 is interpreted as a rare example of a non-brecciated mildly aqueously altered CM chondrite, being similar to clasts within the Paris meteorite (Rubin, 2015), a single clast within the Winchcombe meteorite (Suttle, Daly, et al., 2023) and the Antarctic meteorite EET 96029 (Lee et al., 2016) and LEW 85311 (Lee et al., 2019), but probably more altered than the Asuka CMs (CM2.8-3.0; Kimura et al., 2020). Similar to RKP 17085, Paris is a mildly altered CM2.7 that has gone through thermal metamorphism (300–750°C; Marrocchi et al., 2014). However, Paris has a higher metal content (2 vol%) and contains TCIs. Some less altered clasts in Paris have been classified as 2.9 (Hewins et al., 2014). The Winchcombe meteorite is an unheated CM chondrite breccia with eight different lithologies and subtypes mainly from 2.0 to 2.4. However, a single lithology was assigned a petrologic subtype of 2.6 (named "D" in Suttle, Daly, et al., 2023). Winchcombe's lithology D has undergone more aqueous alteration compared to RKP 17085: pyroxenes in chondrules experienced significant replacement; TCIs are present, as are two generations of calcites (T0 and T1a; Vacher et al., 2017). The existence of multiple ways of determining the degree of aqueous/thermal alteration, and the coexistence of these processes in the same rock, result in classifications that are not necessarily concordant between each other, or chondrites showing differences (e.g., occurrence/lack of TCIs, different calcite generations) with the same petrological subtype. The differences between Paris and RKP 17085 might have not been due to a variation in the aqueous alteration, but, for example, to the intensity of post-hydration thermal metamorphism.

Finally, assuming that the alteration fronts originated in the parent body (see above), their composition, distribution, and relationship to the surrounding chondritic components require explanation in the context of parent body aqueous alteration.

Insights into Early-Stage CM Alteration from RKP 17085

Tracing the alteration fronts across the length of the sample identifies irregular-shaped enclosed regions. The type-A matrix occurs within the enclosed regions, includes most of the chondrules, has a compact, lower porosity texture, and contains euhedral metal grains with minimal evidence of fluid attack, etching, and dissolution. By contrast, the type-B matrix has a higher porosity, being composed of abundant small-scale void space, and includes metal grains with subhedral morphologies which are typically surrounded by haloes of Fe-oxyhydroxides, attesting to partial dissolution and reprecipitation. The alteration fronts themselves record the deposition of Fe^{3+} ions as goethite/ferrihydrite after dissolution from a source region and short-scale transport. Because the type-B matrix is more heavily altered, we argue that the alteration fronts record the migration of fluid from water-rich regions within the (type-B) matrix toward the drier, less altered regions (represented by the type-A matrix). This direction of fluid movement is also consistent with the lobate-cuspate geometry of the fronts. In many instances (e.g., Figure 6a and Figure S2), the alteration fronts terminate at chondrule FGRs suggesting that the FGRs inhibited fluid flow. Furthermore, at the section scale (Figure 1), it can be seen that the alteration fronts enclose multiple separate regions of the matrix. This requires that the multiple different fluid point sources operated and initially evolved in isolation. We can extrapolate from this point to a future, more advanced CM chondrite lithology in which these separate fluid centers expanded sufficiently to link up. These observations support previous arguments for early-stage geochemically isolated microenvironments within the CM lithology (e.g., Palmer & Lauretta, 2011; Pignatelli et al., 2016; Velbel et al., 2012; Verdier-Paoletti et al., 2019), requiring that initial alteration was localized and highly variable in extent.

The way fluids propagate in carbonaceous chondrites —and, therefore, how aqueous alteration progressed, remains poorly constrained (Suttle, King, et al., 2021). One of the critical aspects to understanding the dynamics of alteration is the scale at which fluid flow occurred, either under a limited fluid flow regime (microns to millimeter scale, e.g., Bland et al., 2009; Vacher & Fujiya, 2022) or larger-scale transport (meter to kilometer scale). The latter is mainly supported by numerical models (e.g., Bland & Travis, 2017; Cohen & Coker, 2000; Grimm & McSween, 1989; Travis & Schubert, 2005) and by the recent observations of meter-scale veins (Kaplan et al., 2020) and layered deposits on Bennu (Ishimaru & Lauretta, 2023). What is unique about RKP 17085 is that thanks to the presence of alteration fronts, we can directly reconstruct early fluid propagation processes, moving from the source (presumably melted water-ice grains; Bunch & Chang, 1980; Grimm & McSween, 1989; Le Guillou & Brearley, 2014; McSween Jr, 1979) through a low permeability matrix.

Thermal Metamorphism

The XRD patterns of RKP 17085 indicate that it contains a highly disordered and/or very fine-grained phase, which we interpret as phyllosilicates that were dehydrated by a thermal metamorphic event(s) after the main period of aqueous alteration (King, Schofield, & Russell, 2021). Further evidence for heating comes from the presence of two olivine components in RKP 17085: (i) relatively crystalline, Mg-rich olivine, which we interpret as primary olivine that survived aqueous alteration; and (ii) poorly crystalline and/or fine-grained Fe-rich olivine that recrystallized from dehydrated phyllosilicates during thermal metamorphism (King et al., 2019). As the dehydration of phyllosilicates requires temperatures of ~300–400°C and recrystallization of olivine occurs at temperatures >500°C, we propose that RKP 17085 is a Stage III heated CM chondrite that experienced a peak metamorphic temperature of ~500–750°C (after Nakamura, 2005). Even though part of the matrix recrystallized forming secondary olivine, spectroscopic pointing analysis on the matrix detected features that can be identified as hydrated amorphous silicates (Figure S6b). The absence of a shoulder at 11.3 μm as reported in some cases for Paris (Noun et al., 2019) indicates a very low degree of crystallization.

Although the time scale of post-hydration thermal metamorphism is not well constrained, it was likely short-lived, as has been suggested for other heated CM chondrites based on their mineralogical and chemical properties (e.g., Nakamura, 2005; Nakato et al., 2008; Quirico et al., 2018).

The bulk H_2O content of RKP 17085 estimated from TGA is 9.4 wt% (Figure 3 and Figure S1; Table S1), which is slightly less than the average H_2O content of unheated CM chondrites (~11 wt%) measured using TGA by Garenne et al. (2014), and similar to the Stage II (300–500°C) heated CMs (~9 wt%; King, Schofield, & Russell, 2021). However, as described above, RKP 17085 has been modified by the terrestrial environment. In the TGA data, this is clearly reflected in a mass loss of 8.9 wt % at temperatures <200°C, much higher than most of the CM chondrites previously analyzed using TGA, and of 3.7 wt% between 200 and 400°C due to the breakdown of Fe-oxyhydroxide phases, which again is at the higher end of the range reported for CMs (Garenne et al., 2014; King, Schofield, & Russell, 2021). If we only consider the 400–770°C temperature range (i.e., dehydration of phyllosilicates), the mass loss for RKP 17085 is only

5.7 wt%, which is lower than most unheated CMs and in good agreement with other heated CM chondrites. When combined with the evidence for phyllosilicate dehydration (Figure 3) and partial recrystallization (forming secondary olivine; Figure 2b) as well as the presence of subparallel dehydration cracks in the FGRs (Figure 6a), the evidence for a pronounced post-hydration metamorphic event is clear.

Because Fe-oxyhydroxide minerals (goethite, lepidocrocite, and ferrihydrite) are susceptible to thermal decomposition, the post-hydration metamorphic heating would have affected the appearance and preservation of the alteration fronts in RKP 17085 (considered to have formed before/at the beginning of the thermal metamorphic event[s]). Under vacuum conditions, complete decomposition (loss of the OH budget and recrystallization) is achieved at temperatures between ~220 and 470°C (Kustova et al., 1992; Mitov et al., 2002). The decomposition of Fe-oxyhydroxides forms Fe-oxides, typically wüstite, magnetite, or hematite. Thus, even if the minerals in the alteration fronts suffered complete thermal decomposition, their geochemical signatures and texture in BSE images would be preserved owing to solid-state recrystallization of the Fe-oxyhydroxides as Fe-oxides. However, given the difficulty we had in obtaining coherent Raman or IR spectral signatures from the alteration fronts, we suggest that the former Fe-oxyhydroxides remained at least partially intact, potentially experiencing partial decomposition to form metastable amorphized phases. Furthermore, if metamorphic heating operated under partially closed conditions, the release of H_2O and OH^- from the decomposition of phyllosilicate minerals could have helped stabilize Fe-oxyhydroxide minerals, limiting the extent of their thermal decomposition, as observed for Fe sulfide retention in the CY chondrites (Suttle, Greshake, et al., 2021; Suttle, King, et al., 2023).

Void Space Within the Type-B Matrix

The most likely explanation for the void space found abundantly within the type-B matrix of RKP 17085 is due to the dehydration of hydrated phases during post-hydration metamorphism. In this scenario, the voids would reflect the loss of water, S_2 gas, and CO_2 gas from decomposing phyllosilicate, Fe-sulfide, and carbonate. However, given the mildly aqueously altered nature of RKP 17085, it is also possible that some of the void space within the matrix could represent pores left behind after the loss of an accreted phase. This could be the melting of water-ice grains, or another highly volatile phase (e.g., CO_2-ice or CO-ice grains). Similar tentative evidence of former water-ice grains (with submicron sizes) was suggested for a region within the C2-ung chondrite Acfer 094 (Matsumoto et al., 2019). The CM chondrites accreted relatively high abundances of both water and carbon but low abundances of nitrogen (e.g., Alexander et al., 2013). Recent H-isotope evidence suggests that the direct accretion of water-ice grains into the CM matrix was either unlikely or limited in extent, with most of the water budget instead accreted as pre-hydrated amorphous silicate (Marrocchi et al., 2023). By contrast, the direct accretion of (non-negligible quantities of) C-bearing ices within carbonaceous chondrite matrix is supported by multiple lines of evidence, including (1) the high abundances of carbonate measured in some CM lithologies (up to 4 vol%; Lee et al., 2014), which imply a larger mass balance carbon source than organic matter alone can provide and (2) high CO_2 abundances in CM chondrite fluid inclusions (Tsuchiyama et al., 2021). Under these conditions, sites of former C-ice grains may be expected.

RKP 17085 Within the CM Chondrite Group

The bulk O-isotopic composition of RKP 17085 ($\delta^{17}O = -5.052‰$, $\delta^{18}O = -3.153‰$, $\Delta^{17}O = -3.412‰$; Figure 4) plots away from the main CM group and is, instead, within the CO chondrite field. The bulk O-isotopic composition of RKP 17085 is, therefore, consistent with several other least-altered CMs that have been recently reported, including the Asuka CMs (CM 2.8–3.0; Greenwood et al., 2023; Kimura et al., 2020) and Lewis Cliff (LEW) 85311 (CM2.7; Lee et al., 2019). Collectively, this group provides constraints on the approximate bulk O-isotopic composition of the unaltered anhydrous silicate component accreted by the CM chondrite parent body.

Dehydrated CM chondrites normally show a shift to heavier oxygen isotopic compositions relative to "typical" CMs that only experienced aqueous alteration (Clayton & Mayeda, 1999). However, only minor losses of the light isotopes during dehydroxylation are observed when CMs are exposed to temperatures of ~400°C (Lindgren et al., 2020). In RKP 17085, such enrichment in heavy isotopes is not observed compared to the CM group, possibly because the heating was short lived or occurred at the lower end of Stage III metamorphism, ~500°C.

Finally, the composition of RKP 17085 is slightly offset from the carbonaceous chondrite anhydrous mineral (CCAM) line (as seen in Figure 4) toward the terrestrial fractionation line, consistent with the effects of Antarctic weathering, which results in partial equilibration with Antarctic water (Alexander et al., 2018), conventionally characterized by the standard light Antarctic precipitation (SLAP) composition ($\delta^{17}O$: −29.7‰, $\delta^{18}O$: −55.5‰; Wostbrock et al., 2020). The unusual O-isotopic composition is a result of the complex alteration history and overlapping of mild/moderate events on RKP 17085 parent body and Earth.

IMPLICATIONS

The parent body process forming alteration fronts, being observed in hydrated carbonaceous chondrites subjected to low degrees of aqueous alteration (like the CM 2.7 RKP 17085, the CO3 MIL 07687, and the C2-ungrouped NWA 5958), occurs early in the alteration history and alteration settings dominated by high dissolved Fe^{2+} activities but low Si^{2+} activities. Crucially, the alteration fronts allow the reconstruction of fluid pathways. In RKP 17085 they attest to the existence of multiple distinct fluid point sources, supporting the notion of geochemically isolated microenvironments during the initial stages of hydrothermal activity of carbonaceous chondrites.

CONCLUSIONS

- RKP 17085 is a newly classified mildly aqueously altered CM chondrite, which is unusual for its atypical alteration style (presence of Fe-rich alteration fronts), anomalous O-isotopic composition, and lack of brecciation. Its parent body went through aqueous alteration, followed by a modest thermal event, and terrestrial weathering (preferentially forming Fe-oxyhydroxides in the porous matrix but not affecting most of the metal phase present).
- The Fe-rich alteration fronts in RKP 17085 are resolvable microstructures, even in optical thin section images, and distributed across the sample—making RKP 17085 a rare sample for the study of this feature—evidence of a geologic process of incipient fluid mobilization mechanisms and pathways in CM and CM-related parent bodies in the early stages of aqueous alteration.
- Alteration fronts (and Fe-rich aureoles) are documented in falls (Murray, Murchison) and finds (Antarctica: ALH[A] 81002, MIL 07687, RKP 17085; and Morocco: NWA 5958); (ii) they are found in meteorites with different weathering grades: ALH(A) 81002 and MIL 07687 are severely altered, instead Murray, Murchison, NWA 5958, and RKP 17085—have minor signs of alteration, (iii) and which belong to different groups (CM—mainly, CO, and C2-ungrouped), and (iv) they rarely occur. All factors lead to their extraterrestrial origin.
- The pores within the type-B matrix in RKP 17085 may represent either void space generated by the loss of volatile accretionary ice grains (water-ice or C-bearing ices) and/or space created by the contraction of hydrated minerals during their metamorphic dehydration.

Acknowledgments—Meteorite research at the University of Pisa is supported by the Italian Ministry of Education, University and Research (MIUR) through research grants from the Programma Nazionale delle Ricerche in Antartide (grant number: PNRA16_00029) and The SPaceItUp project funded by the Agenzia Spaziale Italiana (ASI). MDS was funded through a visiting fellow scheme at the University of Pisa, Dipartimento di Scienze della Terra. GP and JRB acknowledge support from Italian Space Agency agreement ASI/INAF 2022-1-HH.0. AJK and HCB acknowledge support from UK Research and Innovation (UKRI) grant number MR/T020261/1. We thank J. Gattacceca, C. Sonzogni, and D. Au Yang for O-isotopic analyses and D. Mauro for assistance during Raman spectroscopy analysis. This research utilizes spectra of meteorites and minerals acquired at the NASA RELAB facility at Brown University. The manuscript benefited of the constructive reviews of M. Lee and an anonymous reviewer, and the careful handling of the associate editor Y. Marrocchi.

Conflict of Interest Statement—The authors of this paper declare that they have no conflict of interest.

Data Availability Statement—The data that support the findings of this study are available in the supplementary material of this article.

Editorial Handling—Dr. Yves Marrocchi

REFERENCES

Abreu, N. M., and Brearley, A. J. 2010. Early Solar System Processes Recorded in the Matrices of Two Highly Pristine CR3 Carbonaceous Chondrites, MET 00426 and QUE 99177. *Geochimica et Cosmochimica Acta* 74: 1146–71.

Alexander, C. M. O'D., Bowden, R., Fogel, M. L., Howard, K. T., Herd, C. D. K., and Nittler, L. R. 2012. The Provenances of Asteroids, and Their Contributions to the Volatile Inventories of the Terrestrial Planets. *Science* 337: 721–23.

Alexander, C. M. O'D., Cody, G. D., De Gregorio, B. T., Nittler, L. R., and Stroud, R. M. 2017. The Nature, Origin and Modification of Insoluble Organic Matter in Chondrites, the Major Source of Earth's C and N. *Chemie der Erde* 77: 227–256.

Alexander, C. M. O'D., Greenwood, R. C., Bowden, R., Gibson, J. M., Howard, K. T., and Franchi, I. A. 2018. A Mutli-Technique Search for the most Primitive CO Chondrites. *Geochimica et Cosmochimica Acta* 221: 406–420.

Alexander, C. M. O'D., Howard, K. T., Bowden, R., and Fogel, M. L. 2013. The Classification of CM and CR Chondrites Using Bulk H, C and N Abundances and Isotopic Compositions. *Geochimica et Cosmochimica Acta* 123: 244–260.

Alexander, C. O. D., Fogel, M., Yabuta, H., and Cody, G. 2007. The Origin and Evolution of Chondrites Recorded in the Elemental and Isotopic Compositions of Their

Macromolecular Organic Matter. *Geochimica et Cosmochimica Acta* 71: 4380–4403.
Alexandre, A., Basile-Doelsch, I., Sonzogni, C., Sylvestre, F., Parron, C., Meunier, J.-D., and Colin, F. 2006. Oxygen Isotope Analyses of Fine Silica Grains Using Laser-Extraction Technique: Comparison with Oxygen Isotope Data Obtained from Ion Microprobe Analyses and Application to Quartzite and Silcrete Cement Investigation. *Geochimica et Cosmochimica Acta* 70: 2827–35.
Amsellem, E., Moynier, F., Mahan, B., and Beck, P. 2020. Timing of Thermal Metamorphism in CM Chondrites: Implications for Ryugu and Bennu Future Sample Return. *Icarus* 339: 113593.
Bates, H. C., King, A. J., Donaldson Hanna, K. L., Bowles, N. E., and Russell, S. S. 2020. Linking Mineralogy and Spectroscopy of Highly Aqueously Altered CM and CI Carbonaceous Chondrites in Preparation for Primitive Asteroid Sample Return. *Meteoritics & Planetary Science* 55: 77–101.
Beck, P., Maturilli, A., Garenne, A., Vernazza, P., Helbert, J., Quirico, E., and Schmitt, B. 2018. What is Controlling the Reflectance Spectra (0.35–150 μm) of Hydrated (and Dehydrated) Carbonaceous Chondrites? *Icarus* 313: 124–138.
Beck, P., Quirico, E., Montes-Hernandez, G., Bonal, L., Bollard, J., Orthous-Daunay, F. R., Howard, K. T., et al. 2010. Hydrous Mineralogy of CM and CI Chondrites from Infrared Spectroscopy and Their Relationship with Low Albedo Asteroids. *Geochimica et Cosmochimica Acta* 74: 4881–92.
Bland, P. A., Jackson, M. D., Coker, R. F., Cohen, B. A., Webber, J. B. W., Lee, M. R., Duffy, C. M., et al. 2009. Why Aqueous Alteration in Asteroids Was Isochemical: High Porosity≠ High Permeability. *Earth and Planetary Science Letters* 287: 559–568.
Bland, P. A., and Travis, B. J. 2017. Giant Convecting Mud Balls of the Early Solar System. *Science Advances* 3: e1602514.
Bland, P. A., Zolensky, M. E., Benedix, G. K., and Sephton, M. A. 2006. Weathering of Chondritic Meteorites. In *Meteorites and the Early Solar System II*, edited by D. S. Lauretta, L. A. Leshin, and H. Y. McSween, Jr., 853–867. Tucson, AZ: The University of Arizona Press.
Braukmüller, N., Wombacher, F., Hezel, D. C., Escoube, R., and Münker, C. 2018. The Chemical Composition of Carbonaceous Chondrites: Implications for Volatile Element Depletion, Complementarity and Alteration. *Geochimica et Cosmochimica Acta* 239: 17–48.
Brearley, A. J. 2012. MIL 07687—An Intriguing, Very Low Petrologic Type 3 Carbonaceous Chondrite with a Unique Style of Aqueous Alteration 43rd Annual Lunar and Planetary Science Conference No. 1659, p. 1233. https://www.lpi.usra.edu/meetings/lpsc2012/pdf/1233.pdf.
Brearley, A. J., and Jones, R. H. 1998. Chondritic Meteorites. In *Planetary Materials*, edited by J. J. Papike, 3-01. Washington, DC: Walter de Gruyter GmbH & Co KG.
Brearley, A. J., Lauretta, D. S., and McSween, H. Y. 2006. The Action of Water. In *Meteorites and the Early Solar System II*, edited by D. S. Lauretta, L. A. Leshin, and H. Y. McSween, Jr., 584–624. Tucson, AZ: The University of Arizona Press.
Browning, L. B., McSween, H. Y., and Zolensky, M. E. 1996. Correlated Alteration Effects in CM Carbonaceous Chondrites. *Geochimica et Cosmochimica Acta* 60: 2621–33.
Bunch, T. E., and Chang, S. 1980. Carbonaceous Chondrites—II. Carbonaceous Chondrite Phyllosilicates and Light Element Geochemistry as Indicators of Parent Body Processes and Surface Conditions. *Geochimica et Cosmochimica Acta* 44: 1543–77.
Burbine, T. H., McCoy, T. J., Meibom, A., Gladman, B., and Keil, K. 2002. Meteoritic Parent Bodies: Their Number and Identification. In *Asteroids III*, edited by W. F. Bottke, 653–668. Tucson, AZ: The University of Arizona Press.
Burgess, R., Wright, I. P., and Pillinger, C. T. 1991. Determination of Sulphur-Bearing Components in C1 and C2 Carbonaceous Chondrites by Stepped Combustion. *Meteoritics* 26: 55–64.
Chan, Q. H., Nakato, A., Kebukawa, Y., Zolensky, M. E., Nakamura, T., Maisano, J. A., Colbert, M. W., et al. 2019. Heating Experiments of the Tagish Lake Meteorite: Investigation of the Effects of Short-Term Heating on Chondritic Organics. *Meteoritics & Planetary Science* 54: 104–125.
Clayton, R. N., and Mayeda, T. K. 1999. Oxygen Isotope Studies of Carbonaceous Chondrites. *Geochimica et Cosmochimica Acta* 63: 2089–2104.
Cohen, B. A., and Coker, R. F. 2000. Modeling of Liquid Water on CM Meteorite Parent Bodies and Implications for Amino Acid Racemization. *Icarus* 145: 369–381.
Cressey, G., and Schofield, P. F. 1996. Rapid Whole-Pattern Profile-Stripping Method for the Quantification of Multiphase Samples. *Powder Diffraction* 11: 35–39.
Dionnet, Z., Aleon-Toppani, A., Baklouti, D., Borondics, F., Brisset, F., Djouadi, Z., Sandt, C., and Brunetto, R. 2018. Organic and Mineralogic Heterogeneity of the Paris Meteorite Followed by FTIR Hyperspectral Imaging. *Meteoritics & Planetary Science* 53: 2608–23.
Garenne, A., Beck, P., Montes-Hernandez, G., Chiriac, R., Toche, F., Quirico, E., Bonal, L., and Schmitt, B. 2014. The Abundance and Stability of "Water" in Type 1 and 2 Carbonaceous Chondrites (CI, CM and CR). *Geochimica et Cosmochimica Acta* 137: 93–112.
Gattacceca, J., McCubbin, F. M., Grossman, J., Bouvier, A., Chabot, N. L., D'Orazio, M., Goodrich, C., et al. 2022. The Meteoritical Bulletin, No. 110. *Meteoritics & Planetary Science* 57: 2102–5.
Greenwood, R. C., Findlay, R., Martins, R., Steele, R. C. J., Shaw, K. M. M., Morton, E., Savage, P. S., et al. 2023. The Formation and Aqueous Alteration of CM2 Chondrites and Their Relationship to CO3 Chondrites: A Fresh Isotopic (O, Cd, Cr, Si, Te, Ti, and Zn) Perspective from the Winchcombe CM2 Fall. *Meteoritics & Planetary Science* 59: 1170–93. https://doi.org/10.1111/maps.13968.
Grimm, R. E., and McSween, H. Y., Jr. 1989. Water and Thermal Evolution of Carbonaceous Chondrite Parent Bodies. *Icarus* 82: 244–280.
Haenecour, P., Floss, C., Brearley, A. J., and Zega, T. J. 2020. The Effects of Secondary Processing in the Unique Carbonaceous Chondrite Miller Range 07687. *Meteoritics & Planetary Science* 55: 1228–56.
Hanna, R. D., Hamilton, V. E., Haberle, C. W., King, A. J., Abreu, N. M., and Friedrich, J. M. 2020. Distinguishing Relative Aqueous Alteration and Heating among CM Chondrites with IR Spectroscopy. *Icarus* 346: 113760.
Hanowski, N. P., and Brearley, A. J. 2000. Iron-Rich Aureoles in the CM Carbonaceous Chondrites Murray, Murchison, and Allan Hills 81002: Evidence for In Situ

Aqueous Alteration. *Meteoritics & Planetary Science* 35: 1291–1308.

Hanowski, N. P., and Brearley, A. J. 2001. Aqueous Alteration of Chondrules in the CM Carbonaceous Chondrite, Allan Hills 81002: Implications for Parent Body Alteration. *Geochimica et Cosmochimica Acta* 65: 495–518.

Hewins, R. H., Bourot-Denise, M., Zanda, B., Leroux, H., Barrat, J. A., Humayun, M., Göpel, C., et al. 2014. The Paris Meteorite, the least Altered CM Chondrite So Far. *Geochimica et Cosmochimica Acta* 124: 190–222.

Howard, K. T., Alexander, C. M. O'D., Schrader, D. L., and Dyl, K. A. 2015. Classification of Hydrous Meteorites (CR, CM and C2 Ungrouped) by Phyllosilicate Fraction: PSD-XRD Modal Mineralogy and Planetesimal Environments. *Geochimica et Cosmochimica Acta* 149: 206–222.

Howard, K. T., Benedix, G. K., Bland, P. A., and Cressey, G. 2009. Modal Mineralogy of CM2 Chondrites by X-Ray Diffraction (PSD-XRD). Part 1: Total Phyllosilicate Abundance and the Degree of Aqueous Alteration. *Geochimica et Cosmochimica Acta* 73: 4576–89.

Howard, K. T., Benedix, G. K., Bland, P. A., and Cressey, G. 2011. Modal Mineralogy of CM Chondrites by X-Ray Diffraction (PSD-XRD): Part 2. Degree, Nature and Settings of Aqueous Alteration. *Geochimica et Cosmochimica Acta* 75: 2735–51.

Ishimaru, K., and Lauretta, D. S. 2023. Analysis of Layered Boulders on Asteroid (101955) Bennu and Their Implications for Fluid Flow on the Parent Body. *Meteoritics & Planetary Science* 59: 193–210.

Jacquet, E., Barrat, J. A., Beck, P., Caste, F., Gattacceca, J., Sonzogni, C., and Gounelle, M. 2016. Northwest Africa 5958: A Weakly Altered CM-Related Ungrouped Chondrite, Not a CI3. *Meteoritics & Planetary Science* 51: 851–869.

Jenkins, L. E., Lee, M. R., Daly, L., King, A. J., Floyd, C. J., Martin, P. E., Almeida, N. V., and Genge, M. J. 2023. Winchcombe: An Example of Rapid Terrestrial Alteration of a CM Chondrite. *Meteoritics & Planetary Science* 59: 988–1005.

Jull, A. J. T., Cheng, S., Gooding, J. L., and Velbel, M. A. 1988. Rapid Growth of Magnesium-Carbonate Weathering Products in a Stony Meteorite from Antarctica. *Science* 242: 417–19.

Kaplan, H. H., Lauretta, D. S., Simon, A. A., Hamilton, V. E., DellaGiustina, D. N., Golish, D. R., Reuter, D. C., et al. 2020. Bright Carbonate Veins on Asteroid (101955) Bennu: Implications for Aqueous Alteration History. *Science* 370: eabc3557.

Kimura, M., Imae, N., Komatsu, M., Barrat, J. A., Greenwood, R. C., Yamaguchi, A., and Noguchi, T. 2020. The Most Primitive CM Chondrites, Asuka 12085, 12169, and 12236, of Subtypes 3.0–2.8: Their Characteristic Features and Classification. *Polar Science* 26: 100565.

King, A., Bates, H. C., Krietsch, D., Busemann, H., Clay, P. M., Schofield, P. N., and Russell, S. S. 2019. The Yamato-Type (CY) Carbonaceous Chondrite Group: Analogues for the Surface of Asteroid Ryugu? *Chemie der Erde* 79: 125531.

King, A., Mason, E. W., Bates, H. C., Schofield, P. F., Donaldson, H. K. L., Bowles, N. E., and Russell, S. S. 2021. Tracing the Earliest Stages of Hydrothermal Alteration on the CM Chondrite Parent Body. *Meteoritics & Planetary Science* 56: 1708–28.

King, A. J., Daly, L., Rowe, J., Joy, K. H., Greenwood, R. C., Devillepoix, H. A., Suttle, M. D., et al. 2022. The Winchcombe Meteorite, a Unique and Pristine Witness from the Outer Solar System. *Science Advances* 8: eabq3925.

King, A. J., Schofield, P. F., Howard, K. T., and Russell, S. S. 2015. Modal Mineralogy of CI and CI-Like Chondrites by X-Ray Diffraction. *Geochimica et Cosmochimica Acta* 165: 148–160.

King, A. J., Schofield, P. F., and Russell, S. S. 2021. Thermal Alteration of CM Carbonaceous Chondrites: Mineralogical Changes and Metamorphic Temperatures. *Geochimica et Cosmochimica Acta* 298: 167–190.

Krietsch, D., Busemann, H., Riebe, M. E., King, A. J., Alexander, C. M. D., and Maden, C. 2021. Noble Gases in CM Carbonaceous Chondrites: Effect of Parent Body Aqueous and Thermal Alteration and Cosmic Ray Exposure Ages. *Geochimica et Cosmochimica Acta* 310: 240–280.

Kustova, G. N., Burgina, E. B., Sadykov, V. A., and Poryvaev, S. G. 1992. Vibrational Spectroscopic Investigation of the Goethite Thermal Decomposition Products. *Physics and Chemistry of Minerals* 18: 379–382.

Le Guillou, C., and Brearley, A. 2014. Relationships between Organics, Water and Early Stages of Aqueous Alteration in the Pristine CR3. 0 Chondrite MET 00426. *Geochimica et Cosmochimica Acta* 131: 344–367.

Lee, M., Lindgren, P., and Sofe, M. R. 2014. Aragonite, Breunnerite, Calcite and Dolomite in the CM Carbonaceous Chondrites: High Fidelity Recorders of Progressive Parent Body Aqueous Alteration. *Geochimica et Cosmochimica Acta* 144: 126–156.

Lee, M. R., and Bland, P. A. 2004. Mechanisms of Weathering of Meteorites Recovered from Hot and Cold Deserts and the Formation of Phyllosilicates. *Geochimica et Cosmochimica Acta* 68: 893–916.

Lee, M. R., Cohen, B. E., King, A. J., and Greenwood, R. C. 2019. The Diversity of CM Carbonaceous Chondrite Parent Bodies Explored Using Lewis Cliff 85311. *Geochimica et Cosmochimica Acta* 264: 224–244.

Lee, M. R., Daly, L., Floyd, C., and Martin, P. E. 2021. CM Carbonaceous Chondrite Falls and Their Terrestrial Alteration. *Meteoritics & Planetary Science* 56: 34–48.

Lee, M. R., Lindgren, P., King, A. J., Greenwood, R. C., Franchi, I. A., and Sparkes, R. 2016. Elephant Moraine 96029, a Very Mildly Aqueously Altered and Heated CM Carbonaceous Chondrite: Implications for the Drivers of Parent Body Processing. *Geochimica et Cosmochimica Acta* 187: 237–259.

Lentfort, S., Bischoff, A., Ebert, S., and Patzek, M. 2021. Classification of CM Chondrite Breccias—Implications for the Evaluation of Samples from the OSIRIS-REx and Hayabusa 2 Missions. *Meteoritics & Planetary Science* 56: 127–147.

Leroux, H., Cuvillier, P., Zanda, B., and Hewins, R. H. 2015. GEMS-Like Material in the Matrix of the Paris Meteorite and the Early Stages of Alteration of CM Chondrites. *Geochimica et Cosmochimica Acta* 170: 247–265.

Lindgren, P., Lee, M. R., Sparkes, R., Greenwood, R. C., Hanna, R. D., Franchi, I. A., King, A. J., et al. 2020. Signatures of the Post-Hydration Heating of Highly Aqueously Altered CM Carbonaceous Chondrites and Implications for Interpreting Asteroid Sample Returns. *Geochimica et Cosmochimica Acta* 289: 69–92.

Lindgren, P., Lee, M. R., Starkey, N. A., and Franchi, I. A. 2017. Fluid Evolution in CM Carbonaceous Chondrites Tracked through the Oxygen Isotopic Compositions of Carbonates. *Geochimica et Cosmochimica Acta* 204: 240–251.

Marrocchi, Y., Gounelle, M., Blanchard, I., Caste, F., and Kearsley, A. T. 2014. The Paris CM Chondrite: Secondary Minerals and Asteroidal Processing. *Meteoritics & Planetary Science* 49: 1232–49.

Marrocchi, Y., Rigaudier, T., Piralla, M., and Piani, L. 2023. Hydrogen Isotopic Evidence for Nebular Pre-Hydration and the Limited Role of Parent-Body Processes in CM Chondrites. *Earth and Planetary Science Letters* 611: 118151.

Martins, Z. 2011. Organic Chemistry of Carbonaceous Meteorites. *Elements* 7: 35–40.

Matsumoto, M., Tsuchiyama, A., Nakato, A., Matsuno, J., Miyake, A., Kataoka, A., Ito, M., et al. 2019. Discovery of Fossil Asteroidal Ice in Primitive Meteorite Acfer 094. *Science Advances* 5: eaax5078.

McAdam, M. M., Sunshine, J. M., Howard, K. T., and McCoy, T. M. 2015. Aqueous Alteration on Asteroids: Linking the Mineralogy and Spectroscopy of CM and CI Chondrites. *Icarus* 245: 320–332.

McSween, H. Y., Jr. 1979. Alteration in CM Carbonaceous Chondrites Inferred from Modal and Chemical Variations in Matrix. *Geochimica et Cosmochimica Acta* 43: 1761–70.

McSween, H. Y., Jr., Sears, D. W., and Dodd, R. T. 1988. Thermal Metamorphism. In *Meteorites and the Early Solar System*, 102–113. Tucson, AZ: The University of Arizona Press.

Mitov, I., Paneva, D., and Kunev, B. 2002. Comparative Study of the Thermal Decomposition of Iron Oxyhydroxides. *Thermochimica Acta* 386: 179–188.

Musolino, A. 2021. Exploring the Variability of Primitive Materials and Processes in the Early Solar System: Characterisation of Four Chondritic Meteorites. Published Masters' Thesis, University of Pisa https://etd.adm.unipi.it/t/etd-05162021-112610/.

Nakamura, T. 2005. Post-Hydration Thermal Metamorphism of Carbonaceous Chondrites. *Journal of Mineralogical and Petrological Sciences* 100: 260–272.

Nakato, A., Nakamura, T., Kitajima, F., and Noguchi, T. 2008. Evaluation of Dehydration Mechanism during Heating of Hydrous Asteroids Based on Mineralogical and Chemical Analysis of Naturally and Experimentally Heated CM Chondrites. *Earth, Planets and Space* 60: 855–864.

Noun, M., Baklouti, D., Brunetto, R., Borondics, F., Calligaro, T., Dionnet, Z., Le Sergeant d'Hendecourt, L., et al. 2019. A Mineralogical Context for the Organic Matter in the Paris Meteorite Determined by a Multi-Technique Analysis. *Life* 9: 44.

Palmer, E. E., and Lauretta, D. S. 2011. Aqueous Alteration of Kamacite in CM Chondrites. *Meteoritics & Planetary Science* 46: 1587–1607.

Peng, Y., and Jing, Y. 2014. Hydrothermal Preparation of Analogous Matrix Minerals of CM Carbonaceous Chondrites from Metal Alloy Particles. *Earth and Planetary Science Letters* 408: 252–262.

Peng, Y., Xi, G., Zhong, C., Wang, L., Lu, J., Sun, X., Zhu, L., et al. 2009. An Experimental Study on the Preparation of Tochilinite-Originated Intercalation Compounds Comprised of Fe1−xS Host Layers and Various Kinds of Guest Layers. *Geochimica et Cosmochimica Acta* 73: 4862–78.

Pignatelli, I., Marrocchi, Y., Vacher, L. G., Delon, R., and Gounelle, M. 2016. Multiple Precursors of Secondary Mineralogical Assemblages in CM Chondrites. *Meteoritics & Planetary Science* 51: 785–805.

Pignatelli, I., Marrocchi, Y., Mugnaioli, E., Bourdelle, F., and Gounelle, M. 2017. Mineralogical, Crystallographic and Redox Features of the Earliest Stages of Fluid Alteration in CM Chondrites. *Geochimica et Cosmochimica Acta* 209: 106–122.

Pommerol, A., Schmitt, B., Beck, P., and Brissaud, O. 2009. Water Sorption on Martian Regolith Analogs: Thermodynamics and Near-Infrared Reflectance Spectroscopy. *Icarus* 204: 114–136.

Prestgard, T., Bonal, L., Eschrig, J., Gattacceca, J., Sonzogni, C., and Beck, P. 2021. Miller Range 07687 and its Place within the CM-CO Clan. *Meteoritics & Planetary Science* 56: 1758–83.

Quirico, E., Bonal, L., Beck, P., Yabuta, H., Nakamura, T., Nakato, A., Flandinet, L., Montagnac, G., Schmitt-Kopplin, P., and Herd, C. D. K. 2018. Prevalence and Nature of Heating Processes in CM and C2-Ungrouped Chondrites as Revealed by Insoluble Organic Matter. *Geochimica et Cosmochimica Acta* 241: 17–37.

Rochette, P., Gattacceca, J., Bonal, L., Bourot-denise, M., Chevrier, V., Clerc, J. P., Consolmagno, G., et al. 2008. Magnetic Classification of Stony Meteorites: 2. Non-Ordinary Chondrites. *Meteoritics & Planetary Science* 43: 959–980.

Rubin, A. E. 2015. An American on Paris: Extent of Aqueous Alteration of a CM Chondrite and the Petrography of its Refractory and Amoeboid Olivine Inclusions. *Meteoritics & Planetary Science* 50: 1595–1612.

Rubin, A. E., Trigo-Rodríguez, J. M., Huber, H., and Wasson, J. T. 2007. Progressive Aqueous Alteration of CM Carbonaceous Chondrites. *Geochimica et Cosmochimica Acta* 71: 2361–82.

Suavet, C., Alexandre, A., Franchi, I. A., Gattacceca, J., Sonzogni, C., Greenwood, R. C., Folco, L., and Rochette, P. 2010. Identification of the Parent Bodies of Micrometeorites with High-Precision Oxygen Isotope Ratios. *Earth and Planetary Science Letters* 293: 313–320.

Suttle, M. D., Daly, L., Jones, R. H., Jenkins, L., Van Ginneken, M., Mitchell, J. T., Bridges, J. C., et al. 2023. The Winchcombe Meteorite—A Regolith Breccia from a Rubble Pile CM Chondrite Asteroid. *Meteoritics & Planetary Science* 59: 1043–67. https://doi.org/10.1111/maps.13938.

Suttle, M. D., Greshake, A., King, A. J., Schofield, P. F., Tomkins, A., and Russell, S. S. 2021. The Alteration History of the CY Chondrites, Investigated through Analysis of a New Member: Dhofar 1988. *Geochimica et Cosmochimica Acta* 295: 286–309.

Suttle, M. D., King, A. J., Harrison, C. S., Chan, Q. H. S., Greshake, A., Bartoschewitz, R., Tomkins, A. G., Salge, T., Schofield, P. F., and Russell, S. S. 2023. The Mineralogy and Alteration History of the Yamato-Type (CY) Carbonaceous Chondrites. *Geochimica et Cosmochimica Acta* 361: 245–264.

Suttle, M. D., King, A. J., Ramkissoon, N. K., Bonato, E., Franchi, I. A., Malley, J., Schofield, P. F., Najorka, J., Salge, T., and Russell, S. S. 2022. Alteration Conditions on the CM and CV Parent Bodies—Insights from Hydrothermal Experiments with the CO Chondrite Kainsaz. *Geochimica et Cosmochimica Acta* 318: 83–111.

Suttle, M. D., King, A. J., Schofield, P. F., Bates, H., and Russell, S. S. 2021. The Aqueous Alteration of CM Chondrites, a Review. *Geochimica et Cosmochimica Acta* 299: 219–256.

Takir, D., Emery, J. P., Mcsween, H. Y., Hibbitts, C. A., Clark, R. N., Pearson, N., and Wang, A. 2013. Nature

and Degree of Aqueous Alteration in CM and CI Carbonaceous Chondrites. *Meteoritics & Planetary Science* 48: 1618–37.
Takir, D., Stockstill-Cahill, K. R., Hibbitts, K., and Nakauchi, Y. 2019. 3-μm Reflectance Spectroscopy of Carbonaceous Chondrites under Asteroid-like Conditions. *Icarus* 333: 243–251.
The Meteoritical Bulletin 2023. Online. August 29, 2023 https://www.lpi.usra.edu/meteor/.
Tonui, E., Zolensky, M., Hiroi, T., Nakamura, T., Lipschutz, M. E., Wang, M.-S., and Okudaira, K. 2014. Petrographic, Chemical and Spectroscopic Evidence for Thermal Metamorphism in Carbonaceous Chondrites I: CI and CM Chondrites. *Geochimica et Cosmochimica Acta* 126: 284–306.
Travis, B. J., and Schubert, G. 2005. Hydrothermal Convection in Carbonaceous Chondrite Parent Bodies. *Earth and Planetary Science Letters* 240: 234–250.
Trigo-Rodríguez, J. M., Rimola, A., Tanbakouei, S., Soto, V. C., and Lee, M. 2019. Accretion of Water in Carbonaceous Chondrites: Current Evidence and Implications for the Delivery of Water to Early Earth. *Space Science Reviews* 215: 1–27.
Trigo-Rodríguez, J. M., and Rubin, A. E. 2006. Evidence for Parent-Body Aqueous Flow in the MET 01070 CM Carbonaceous Chondrite. *37th Lunar and Planetary Science Conference*, No. 1104.
Tsuchiyama, A., Miyake, A., Okuzumi, S., Kitayama, A., Kawano, J., Uesugi, K., Takeuchi, A., Nakano, T., and Zolensky, M. 2021. Discovery of Primitive CO_2-bearing Fluid in an Aqueously Altered Carbonaceous Chondrite. *Science Advances* 7: eabg9707.
Vacher, L. G., and Fujiya, W. 2022. Recent Advances in our Understanding of Water and Aqueous Activity in Chondrites. *Elements* 18: 175–180.
Vacher, L. G., Marrocchi, Y., Villeneuve, J., Verdier-Paoletti, M. J., and Gounelle, M. 2017. Petrographic and C & O Isotopic Characteristics of the Earliest Stages of Aqueous Alteration of CM Chondrites. *Geochimica et Cosmochimica Acta* 213: 271–290.
Vacher, L. G., Piani, L., Rigaudier, T., Thomassin, D., Florin, G., Piralla, M., and Marrocchi, Y. 2020. Hydrogen in Chondrites: Influence of Parent Body Alteration and Atmospheric Contamination on Primordial Components. *Geochimica et Cosmochimica Acta* 281: 53–66.
Vacher, L. G., Piralla, M., Gounelle, M., Bizzarro, M., and Marrocchi, Y. 2019. Thermal Evolution of Hydrated Asteroids Inferred from Oxygen Isotopes. *The Astrophysical Journal* 882: L20.
Vacher, L. G., Truche, L., Faure, F., Tissandier, L., Mosser-Ruck, R., and Marrocchi, Y. 2019. Deciphering the Conditions of Tochilinite and Cronstedtite Formation in CM Chondrites from Low Temperature Hydrothermal Experiments. *Meteoritics & Planetary Science* 54: 1870–89.
Van Ginneken, M., Genge, M. J., Folco, L., and Harvey, R. P. 2016. The Weathering of Micrometeorites from the Transantarctic Mountains. *Geochimica et Cosmochimica Acta* 179: 1–31.
Velbel, M. A. 1988. The Distribution and Significance of Evaporitic Weathering Products on Antarctic Meteorites. *Meteoritics* 23: 151–59.
Velbel, M. A., Tonui, E. K., and Zolensky, M. E. 2012. Replacement of Olivine by Serpentine in the Carbonaceous Chondrite Nogoya (CM2). *Geochimica et Cosmochimica Acta* 87: 117–135.
Verdier-Paoletti, M. J., Marrocchi, Y., Vacher, L. G., Gattacceca, J., Gurenko, A., Sonzogni, C., and Gounelle, M. 2019. Testing the Genetic Relationship between Fluid Alteration and Brecciation in CM Chondrites. *Meteoritics & Planetary Science* 54: 1692–1709.
Wostbrock, J. A. G., Cano, E. J., and Sharp, Z. D. 2020. An Internally Consistent Triple Oxygen Isotope Calibration of Standards for Silicates, Carbonates and Air Relative to VSMOW2 and SLAP2. *Chemical Geology* 533: 119432.
Zolensky, M. E., Mittlefehldt, D. W., Lipschutz, M. E., Wang, M. S., Clayton, R. N., Mayeda, T. K., Grady, M. M., Pillinger, C., and David, B. 1997. CM Chondrites Exhibit the Complete Petrologic Range from Type 2 to 1. *Geochimica et Cosmochimica Acta* 61: 5099–5115.

SUPPORTING INFORMATION

Additional supporting information may be found in the online version of this article.

Figure S1. TGA plots with mass loss and DTG curve for RKP 17085 (samples a and b). Colored areas highlight the range as reported in Table S1.

Figure S2. X-ray map of RKP 17085 showing the mobilization of Fe in the fronts and distribution of other components (carbonates, sulfides, CAIs). Colors legend: Fe = yellow, Ni = blue, S = green, Mg = pink, Ca = red, Si = violet, Al = gray.

Figure S3. (a) BSE images of an RKP 17085's compound chondrule with unaltered anhydrous silicates (pure forsterite and enstatite) and altered mesostasis (a close-up image in b).

Figure S4. BSE images of RKP 17085. For each image, the position within the thin section is indicated in the upper left corner (take Figure 1b as a reference). (a) A large unaltered kamacite grain (Kam) with a fragment of forsterite (with variable composition from the core to the rim Fo_{85-66}) and a T0 calcite (Cal). (b) An anhedral T0 calcite (Cal) grain. (c) Needle crystals inside the alteration front and (d) in the external surface (green arrow), with other weathering phases (Fe-oxides). (e) Encrustation of Fe-oxyhydroxides (red arrows) that enter the meteorite from the external surface (left to right), with their typical layered texture (f), and in the proximity of the fusion crust.

Figure S5. Raman spectra of Ca-carbonate grains in RKP 17085 (red and yellow spectra) identified as calcite (black reference spectra from RRUFF database).

Figure S6. IR spectra resulting from maps of alteration fronts, matrix, and needles in RKP 17085. (a) Optical image of reference for the spectra in the following figures (the rectangle at the bottom left represents the spatial resolution for the IR measurements, centered on the position indicated by the circles). (b) Four different collective spectra of matrix (each spectrum is an average of the spots in the areas in [a]) plus their global average

(Global Avg) are compared: all of them have a strong Si-O stretching band at 10 μm, and the OH absorbance band at 2.75 μm, which can be due to hydrated amorphous silicates (Dionnet et al., 2018; Noun et al., 2019). (c) The spectra of two different needles are compared to the matrix and goethite ("JB-JLB-H58-B" of the RELAB database). The dotted lines refer to "needle spot n.2" and are consistent with the presence of goethite; the arrows are bands in "needle spot n.1" that indicate the presence of other Fe-hydroxides (according to Noun et al., 2019). (d) Comparison of matrix and (alteration) front spectra: no significant differences are observed. Light green dotted lines indicate the presence of amorphous silicates and the dark green dotted lines Fe-oxyhydroxides.

Figure S7. Example of Raman spectra from the two different matrix regions in RKP 17085 showing profiles of the G and D bands.

Table S1. Results from TGA analyses of two samples of RKP 17085 (aliquots a and b).

Table S2. Bulk O-isotope compositions of RKP 17085 and other chondrites with fronts (NWA 5958, MIL 07687), the CMs Asuka (A-12169, A-12236, A-12085) with very low aqueous alteration described in Kimura et al. (2020) and Greenwood et al. (2023), and the CO3 Kainsaz—in which fronts have been experimentally produced (Suttle et al., 2022).

Table S3. Chemical analyses in weight %, with average and standard deviation (σ) for matrix TA, matrix TB, alteration fronts, needles, and chondrules mesostasis, respectively, in RKP 17085 (Figure 5).

Table S4. Olivine chemical compositions in chondrules (c) and fragments (f) of RKP 17085 (oxides wt % normalized to 100% by EDS; Musolino, 2021).

Table S5. Low-Ca and high-Ca pyroxenes chemical compositions in chondrules (c) and fragments (f) of RKP 17085 (oxides wt% normalized to 100% by EDS; Musolino, 2021).